University of Groningen

Kinome directed target discovery and validation in unique ovarian clear cell carcinoma models
Caumanns, Joost

Publication date:
2019

[Link to publication in University of Groningen/UMCG research database](#)

CHAPTER 4

Integrative kinome profiling identifies mTORC1/2 inhibition as treatment strategy in ovarian clear cell carcinoma

Joseph J. Caumanns[1], Katrien Berns[5], G. Bea A. Wisman[1], Rudolf S.N. Fehrmann[2], Tushar Tomar[1], Harry Klip[1†], Gert J. Meersma[1], E. Marielle Hijmans[5], Annemiek M.C. Gennissen[5], Evelien W. Duiker[3], Desiree Weening[4], Hiroaki Itamochi[6], Roelof J.C. Kluin[5], Anna K.L. Reyners[2], Michael J. Birrer[7], Helga B. Salvesen[8†], Ignace Vergote[9], Els van Nieuwenhuysen[9], James Brenton[10], E. Ioana Braicu[11], Jolanta Kupryjanczyk[12], Beata Spiewankiewicz[13], Lorenza Mittempergher[5], René Bernards[5], Ate G.J. van der Zee[1] and Steven de Jong[2]

[1]Department of Gynecologic Oncology, [2]Department of Medical Oncology, [3]Department of Pathology and Medical Biology and [4]Department of Genetics, Cancer Research Center Groningen, University Medical Center Groningen, University of Groningen, Hanzeplein 1, 9713 GZ Groningen, the Netherlands. [5]Division of Molecular Carcinogenesis, the Netherlands Cancer Institute, Plesmanlaan 121, 1066 CX Amsterdam, the Netherlands. [6]Department of Obstetrics and Gynecology, Iwate Medical University School of Medicine, Morioka, Iwate 020-8505, Japan. [7]Center for Cancer Research, The Gillette Center for Gynecologic Oncology, Massachusetts General Hospital, Harvard Medical School, 32 Fruit Street, Boston, MA 02114, United States. [8]Department of Obstetrics and Gynecology, Haukeland University Hospital, N5021 Bergen, Norway. [9]Department of Gynaecology and Obstetrics, Leuven Cancer Institute, University Hospitals Leuven, Herestraat 49, 3000 Leuven, Belgium. [10]Cancer Research UK Cambridge Research Institute, Li Ka Shing Centre, Robinson Way, Cambridge CB2 0RE, UK. [11]Department of Gynecology, Charité Medical University, Augustenburger Platz 1, 13353 Berlin, Germany. [12]Department of Pathology and Laboratory Diagnostics, and [13]Department of Gynecologic Oncology, Maria Sklodowska-Curie Memorial Cancer Center and Institute of Oncology, Roentgena 5, 02-781, Warsaw, Poland.

† in memory of

Integrative kinome profiling identifies mTORC1/2 inhibition as treatment strategy in ovarian clear cell carcinoma

Joseph J. Caumanns, Katrien Berns, G. Bea A. Wisman, Rudolf S.N. Fehrmann, Tushar Tomar, Harry Klip, Gert J. Meersma, E. Marielle Hijmans, Annemiek M.C. Gennissen, Evelien W. Duiker, Desiree Weening, Hiroaki Itamochi, Roelof J.C. Kluin, Anna K.L. Reyners, Michael J. Birrer, Helga B. Salvesen†, Ignace Vergote, Els van Nieuwenhuysen, James Brenton, E. Ioana Braicu, Jolanta Kupryjanczyk, Beata Spiewankiewicz, Lorenza Mittempergher, René Bernards, Ate G.J. van der Zee and Steven de Jong

Advanced stage ovarian clear cell carcinoma (OCCC) is unresponsive to conventional platinum-based chemotherapy. Frequent alterations in OCCC include deleterious mutations in the tumor suppressor *ARID1A* and activating mutations in the PI3K subunit *PIK3CA*. In this study, we aimed to identify currently unknown mutated kinases in OCCC patients and test druggability of downstream affected pathways in OCCC models. In a large set of OCCC patients (n=124), the human kinome (518 kinases) and additional cancer related genes were sequenced and copy number alterations were determined. Genetically characterized OCCC cell lines (n=17) and OCCC patient-derived xenografts (n=3) were used for drug testing of ERBB tyrosine kinase inhibitors erlotinib and lapatinib, the PARP inhibitor olaparib and the mTORC1/2 inhibitor AZD8055. We identified several putative driver mutations in kinases at low frequency that were not previously annotated in OCCC. Combining mutations and copy number alterations, 91% of all tumors are affected in the PI3K/AKT/mTOR pathway, the MAPK pathway or the ERBB family of receptor tyrosine kinases and 82% in the DNA repair pathway. Strong p-S6 staining in OCCC patients suggests high mTORC1/2 activity. We consistently found that the majority of OCCC cell lines are especially sensitive to mTORC1/2 inhibition by AZD8055 and not towards drugs targeting ERBB family of receptor tyrosine kinases or DNA repair signaling. We subsequently demonstrated the efficacy of mTORC1/2 inhibition in all our unique OCCC patient-derived xenograft models. These results propose mTORC1/2 inhibition as an effective treatment strategy in OCCC.

TRANSLATIONAL RELEVANCE

Advanced stage ovarian clear cell carcinoma (OCCC) is less responsive to platinum-based chemotherapy compared to high-grade serous ovarian carcinoma. Our in-depth analyses of a large set of OCCC patients reveal numerous genomic alterations related to activation of mTORC1/2. High sensitivity, especially to inhibitors targeting both mTORC1 and mTORC2 is observed in a large OCCC cell line panel. Similar results are obtained in OCCC patient-derived xenografts, signifying the clinical implications of these genomic alterations. Targeting of mTORC1 in combination with standard chemotherapy did not improve overall survival in OCCC patients. Therefore, mTORC1/2 inhibitors, currently evaluated in phase II clinical trials, are proposed for the treatment of OCCC. Based on the mutational landscape

in OCCC, our in vitro results and the toxicity observed with dual inhibitors of PI3K and mTORC1/2, future treatment combinations of mTORC1/2 inhibitors with either PI3K or MEK inhibitors could be considered to improve clinical benefit for OCCC patients.

INTRODUCTION

In the United States, ovarian cancer is the fifth-leading cause of cancer deaths in women (1). Ovarian clear cell carcinoma (OCCC) is the second most common subtype of epithelial ovarian cancer. The majority of OCCC patients are diagnosed at an early stage (57-81% at stage I/II) and have better overall survival compared to stage matched high-grade serous (HGS) ovarian cancer, the most common subtype of ovarian cancer. In contrast, OCCC patients diagnosed at late stage respond poorly to standard platinum-based chemotherapy compared to late stage HGS ovarian carcinoma patients (2). In recent years, genetic studies in relatively small patient groups have revealed the mutational landscape in OCCC. The SWI-SNF chromatin remodeling complex DNA binding AT-rich interactive domain 1A gene (*ARID1A*) has been shown to be deleteriously mutated in 40-57% of OCCC patients, the highest percentage found in any cancer (3, 4). Loss of ARID1A protein, being a key component of the complex, may affect the expression of many genes (5). Activation of the PI3K/AKT/mTOR pathway, implicated in survival, protein synthesis and proliferation, is another major player in OCCC. *PIK3CA*, encoding the catalytic domain of PI3K, contains activating mutations in 30-40% of OCCC patients, whereas expression of the PI3K antagonist PTEN is diminished in 40% of OCCC patients (4, 6, 7). Furthermore, mutations in the oncogene *KRAS* and the tumor suppressor gene *TP53* have been identified in 4.7%-14% and 10%-15% of

OCCC patients, respectively (1, 4, 6, 8, 9). In addition to mutational aberrations, copy number alterations (CNA) have been found in OCCC tumor samples in the proto oncogene *ZNF217*, tumor suppressor genes, cyclin dependent kinase inhibitors *CDKN2A* and *CDKN2B* and the membrane receptor oncogene *MET* (10-12).

The identification of the most frequently mutated genes *ARID1A* and *PIK3CA* may lead to new therapeutic strategies. In particular, the effects of ARID1A loss are being investigated and vulnerabilities in *ARID1A* mutant cancers are being identified. Synthetic lethal interactions have recently been demonstrated in *ARID1A* mutant OCCC cancer cell lines by shRNA mediated suppression of *ARID1B*, a homolog of *ARID1A*, as well as chemical inhibition of the histone H3 methyltransferase EZH2 and histone deacetylase HDAC6 (13-15). PI3K signaling-mediated tumor addiction through the well-studied hypermorphic mutant forms of *PIK3CA* (E545* and H1047*) was studied extensively in multiple cancer types including OCCC. Recent translational research in OCCC cell lines demonstrated sensitivity to PI3K/mTOR dual inhibitors and AKT inhibitors, although *PIK3CA* mutations did not predict sensitivity to these inhibitors (16, 17).

In the present study, we aimed to identify novel targetable mutations by means of high-coverage sequencing of all protein kinase genes, referred to as the kinome, and of a subgroup of cancer-related genes in a large set of OCCC. In addition, we determined copy number gains and losses in kinases and other genes of OCCC tumors using high-coverage single nucleotide polymorphism (SNP) arrays. To detect kinase mutations and CNA at both high and low frequency, we used a large cohort of 124 untreated primary OCCC tumors and most of the available OCCC cell lines (n=17). Finally, we
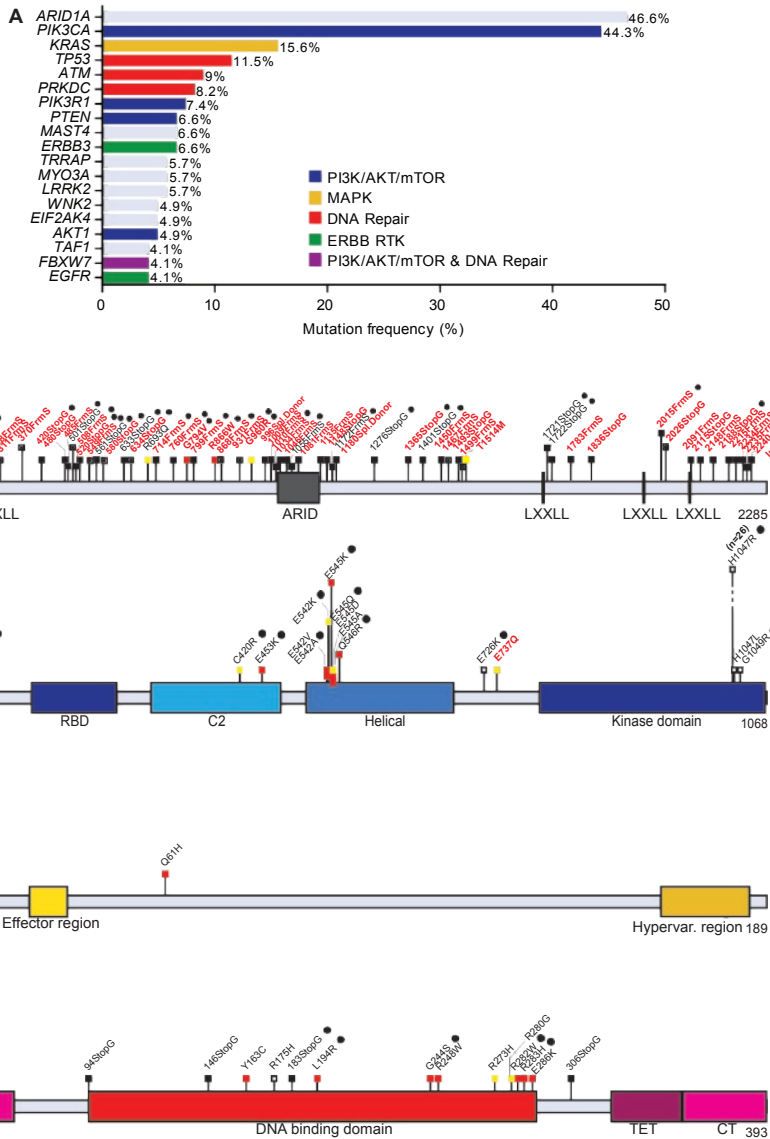
Figure 1 | Most frequent OCCC mutations. (A) Frequently mutated genes in OCCC as identified by kinome sequencing in 122 OCCC tumors using a 4% cutoff. *ARID1A* mutations (n=54 tumors) were revealed using haloplex sequencing on 116 OCCC tumors. Mutated genes involved in PI3K (*PIK3CA*, *PIK3R1*, *PTEN*, *AKT1* and *FBXW7*, n=54, n=9, n=8, n=6, n=5 tumors, respectively), MAPK (*KRAS*, n=19 tumors), or DNA repair signaling (*TP53*, *ATM*, *PRKDC* and *FBXW7*, n=14, n=11, n=10 and n=5 tumors, respectively) and ERBB family of receptor tyrosine kinases (*ERBB3* and *EGFR*, n=8 and n=5 tumors) are among the frequently mutated genes. Schematics of identified mutations in known OCCC mutated genes **(B)** *ARID1A*, **(C)** *PIK3CA*, **(D)** *KRAS* and **(E)** *TP53*. Mutation marks are shown in black (truncating), red (SIFT and PolyPhen damaging prediction), yellow (SIFT or PolyPhen damaging prediction) or white (SIFT and PolyPhen benign prediction). Mutation effects are indicated with a black spot when paired control was available and written in black (previously described mutation) or red (novel mutations).

functionally validated several candidate targets in OCCC cell lines and unique OCCC patient-derived xenograft (PDX) models. Our results indicate mTORC1/2 inhibition as an approach to guide future development of therapeutic strategies for OCCC.

RESULTS

Kinome sequencing analysis

Across all OCCC tumors (n=122) and OCCC cell lines (n=17), 95.9% of all bases had >20 read coverage for variant calling. The mean coverage depth for aligned reads was 99.3x. On average 1.17% of the sequenced genes were mutated per patient. Genes with a high mutation frequency (>4%) across all OCCC tumors are shown in Figure 1A. Re-sequencing of these 19 genes using Haloplex confirmed 227 out of the 234 mutations (97%) that were originally identified by kinome sequencing using the same tumor DNA. The majority of genes with a high mutation frequency are implicated in well-known cancer related pathways like the PI3K/AKT/mTOR pathway (*PIK3CA*, *PTEN*, *PIK3R1* and *AKT1*), MAPK signaling transduction pathway (*KRAS*), DNA repair pathway (*TP53*, *ATM* and *PRKDC*), ERBB family of receptor tyrosine kinase genes (*ERBB3* and *EGFR*) and chromatin remodeling genes (*ARID1A*). The frequencies of previously described mutated genes observed in our study were in agreement with such frequencies reported earlier in smaller studies of OCCC (Fig. 1A) (3, 4, 6, 8, 9).

ARID1A mutations were analyzed using Haloplex sequencing only. Out of 54 *ARID1A* mutant tumors, 18 tumors contained homozygous frameshift or stop-gain mutations, 13 tumors harbored more than one heterozygous mutation, while 23 tumors contained a single heterozygous frameshift or stop-gain mutation (Fig. 1B). The identified proportion of each type of mutation in *ARID1A* matches those reported in earlier studies (3, 4). *ARID1A* mutant and wild type tumors did not show differential mutation incidence in kinome genes (7.4 vs. 6.6 mutations per tumor on average).

Statistical binomial univariate testing of all 851 identified kinome mutations revealed 11 significantly mutated genes (p<0.05) relative to background mutations. These predicted oncogenic drivers were *PIK3CA*, *KRAS*, *TP53*, *PTEN*, *AKT1*, *PIK3R1*, *FBXW7*, *ERBB3*, *ATM*, *CHEK2* and *MYO3A* (Supplementary Table 3). *PIK3CA* and *KRAS* exhibited mutations in established hotspot sites in aa Q542, Q545 and H1047 in *PIK3CA* and G12 in *KRAS*, while *TP53* mutations were distributed across the *TP53* DNA binding domain (Fig. 1C-E).

Interestingly, we identified mutations in three genes not previously described in OCCC (*AKT1*, *PIK3R1* and *ERBB3*) and with an established role in PI3K/AKT/mTOR pathway activation. *AKT1* missense mutations were identified in six tumors (4.9%). AKT1 is one of the key components of the PI3K/AKT/mTOR cascade. The PH domain of AKT1 interacts with its kinase domain and maintains the protein in a closed and inactive state (18). One candidate somatic mutation, D323N, was located in the kinase domain. The mutations R25H, L52R (occurring in three tumors) and W80R (both described in COSMIC) were all located in the *AKT1* PH domain (Supplementary Fig. 2A). *PIK3R1* was mutated in nine tumors (7.3%), of which seven tumors carried mutations in the inter-SH2-1 SH2-2 domain of the protein (aa 429-623). This domain binds PIK3CA and is required for the inhibitory role of PIK3R1 on PIK3CA (19). Two of the inter-SH2 domain mutations are described in COSMIC: E439* and T576* in-frame deletions. In addition, we identified six novel inter-SH2 domain mutations; two somatic missense (aa

4

N453D and T471S, together in one tumor), two somatic in-frame deletions (aa QF455* and RE461*), one candidate somatic frameshift (starting in aa 582) and one candidate somatic stop-gain mutation (aa 571) (Supplementary Fig. 2B). In *ERBB3* we identified 10 missense mutations across eight distinct tumors (5.7%). At the cell membrane ERBB3 can dimerize with other ERBB family members and regulate downstream kinase signaling. Six mutations were located across the extracellular domains of *ERBB3* and two could be identified as somatic. The D297Y mutation has been described as a hotspot location in ovarian and colorectal cancer (20). Furthermore, three mutations were in the intracellular C-terminal domain and one in the kinase domain (Supplementary Fig. 2C). Of the other significantly mutated genes, F-Box and WD Repeat Domain Containing 7 (*FBXW7*) has been assigned a role in PI3K regulation and DNA repair. These mutations are mainly found in its WD repeats (21). ATM Serine/Threonine Kinase (*ATM*) and Checkpoint kinase 2 (*CHEK2*) are designated as DNA repair genes whereas Myosin IIIA (*MYO3A*) is an actin-dependent motor protein. Mutations in *FBXW7* and *ATM* were previously described in OCCC (Supplementary Fig. 2D-G) (22).

Pathway analysis of kinome mutations

We also investigated the pathways in which genes with a high mutation frequency are involved. To this end, all low mutation frequency genes (<4%) present in PI3K/AKT/mTOR, MAPK and DNA repair pathways, the ERBB family of receptor tyrosine kinases and mutations in *ARID1A* were mapped per tumor in order to determine mutational spectra across these signaling pathways in OCCC. One or more mutations were found in PI3K/AKT/mTOR pathway genes in 76 patients (62.3%), in MAPK pathway genes in 22 patients (18%),

in the ERBB family of receptor tyrosine kinases in 18 patients (14.8%) and in DNA repair pathway genes in 46 patients (37.7%). The co-occurrence of mutations in both *ARID1A* and *PIK3CA* in this large set of OCCC tumors was in accordance with the findings from a previous, smaller study (Supplementary Fig. 3A) (4, 23). *PIK3R1* mutations were mutually exclusive with *PIK3CA* mutant tumors (*p*=0.043) and a trend was observed for *PTEN* with *PIK3CA* mutant tumors (*p*=0.0756). In general, *TP53* mutant tumors (including pure OCCCs) were mutually exclusive with both *ARID1A* and *PIK3CA* mutant tumors (*p*=0.0031), in agreement with previous literature (5). Surprisingly, co-occurrence of *TP53* and *ARID1A* or *PIK3CA* mutations was observed in a few cases. In total 108 out of 122 tumors (89%) comprised one or more mutations in genes belonging to the PI3K/AKT/mTOR pathway, MAPK pathway, DNA repair pathway and ERBB family of receptor tyrosine kinases (Supplementary Fig. 3A).

Evidently, there is a large overlap in tumors that were both *ARID1A* mutant and harbored a mutation in DNA repair genes or PI3K/AKT/mTOR, MAPK and ERBB family of receptor tyrosine kinase genes (Supplementary Fig. 3B). Subdividing tumors into *ARID1A* heterozygous-mutated and homozygous-mutated tumors did not change the overlap in mutations in PI3K/AKT/mTOR, MAPK, and ERBB family of receptor tyrosine kinase genes or DNA repair genes in both groups (data not shown). *ARID1A* wild type tumors more frequently contained mutations in DNA repair genes in addition to mutations in PI3K/AKT/mTOR, MAPK or the ERBB family of receptor tyrosine kinase genes as compared to *ARID1A* mutant tumors (49% vs. 26%, *p*=0.0385).

CNA analysis
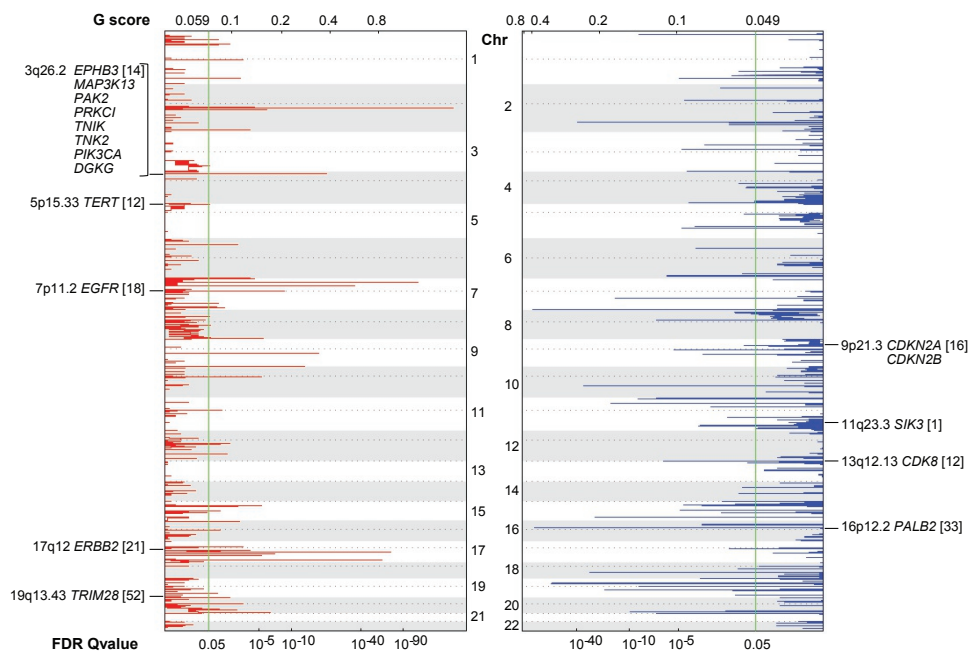
In 108 SNP genotyped primary OCCC

Figure 2 | Kinase CNA in OCCC. Significant CNA in kinases across 108 OCCC tumors as determined by GISTIC analysis. All kinases and cancer related genes from the kinome sequencing gene panel that were focally significantly amplified (red) or deleted (blue) are vertically indicated along the chromosomes. Chromosomal location and total amount of tumors (between brackets) harboring the event are annotated with each gene name. The false-discovery rate (FDR) (0.05 threshold), indicated by the green line, and G-score are shown along the horizontal axis.

tumors, genomic identification of significant targets in cancer (GISTIC) analysis annotated 324 significantly amplified genes located in 48 focal regions. We identified amplification of *ZNF217* (20q13.20), a transcriptional regulator previously described in OCCC (11), in 29 tumors (27%, *p*=0.014). Using GISTIC analysis, we subsequently found multiple kinases and other cancer-related genes among the significantly amplified genes (Fig. 2).

One recurrently amplified region (3q26.2) contained multiple kinases; *PIK3CA*, *EPHB3*, *MAPK3K13*, *PAK2*, *PRKCI*, *TNIK*, *TNK2* and *DGKG* (14 tumors, 13%, *p*=0.046). The cancer-related gene *TERT* (5p15.33), included in kinome sequencing, was amplified in 12 tumors (11%, *p*=0.044). *EGFR*

(7p11.2) emerged as the most significant recurrently amplified kinase; it was present in 18 OCCC tumors (17%, *p*<0.0001). Other recurrently amplified kinases included *ERBB2* (17q12), which was amplified in 21 tumors (19%, *p*=0.002), and the chromatin-associated and transcriptional control-related kinase *TRIM28* (19q13.43), which was amplified in 52 tumors (48%, *p*=0.0035).

Furthermore, a total of 118 significantly deleted genes were identified in 62 focally deleted regions. Two significantly deleted kinases could be identified: *SIK3* (11q23.3) and the transcriptional repressor *CDK8* (13q12.13) (Fig. 2). In addition, three known cancer related genes included in kinome sequencing were significantly deleted. The cell cycle regulators *CDKN2A* and *CDKN2B* (both
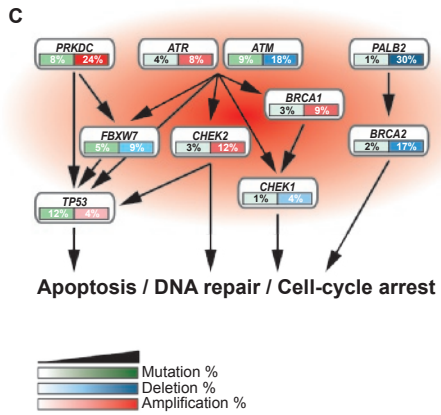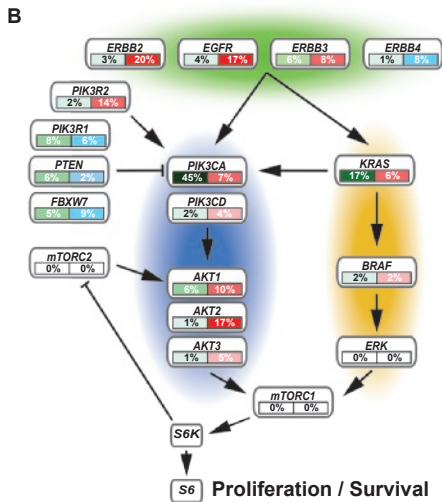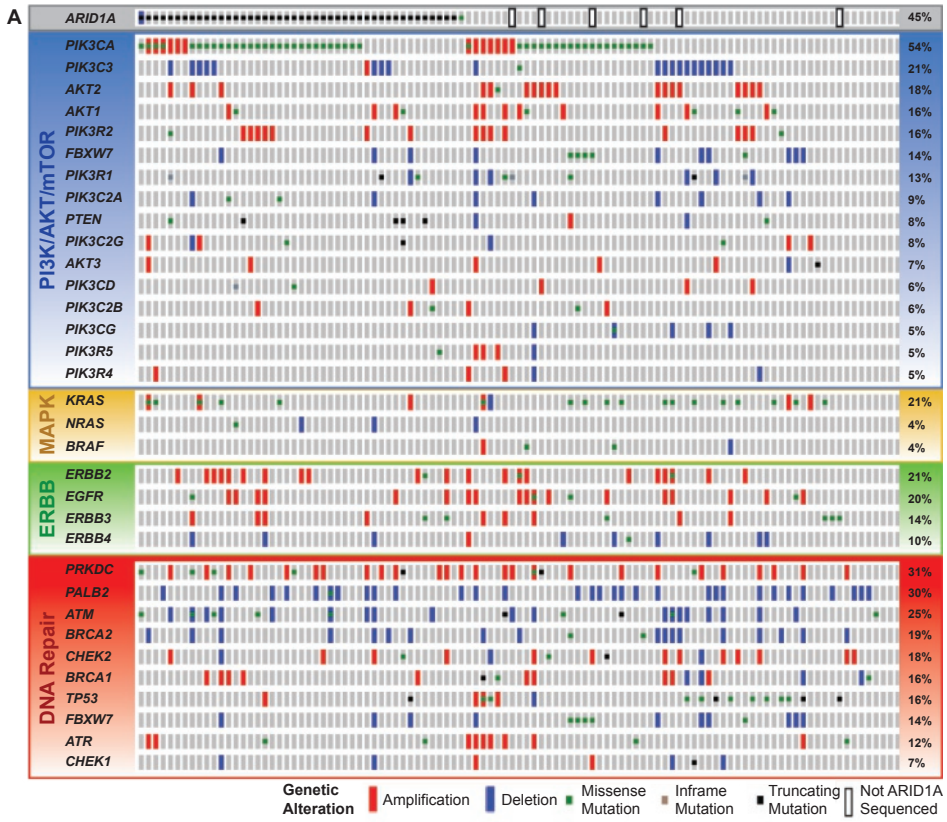
Figure 3 | Mutation and CNA distribution. (A) Nonsynonymous mutation distribution in genes involved in the frequently mutated PI3K/AKT/mTOR (blue), MAPK pathway (yellow), the ERBB family of receptor tyrosine kinases (green) and DNA repair pathway (red) as well as *ARID1A* and *PALB2* are shown with On-

coPrint. CNA for each mutated gene are added. The 106 OCCC tumors that were both kinome sequenced and SNP arrayed are shown on the horizontal axis ordered on total event frequency in the subsequently altered pathways. **(B)** The interacting ERBB family of receptor tyrosine kinases, PI3K/AKT/mTOR and MAPK pathway and **(C)** DNA repair pathway are commonly altered. These alterations are defined by mutations and CNA.

located on 9p21.3) were deleted in 16 tumors (15%, p=0.024) and *PALB2* (16p12.2), an essential chaperone of *BRCA2*, was deleted in 33 tumors (31%, p<0.0001).

A separate GISTIC analysis was implemented to compare *ARID1A* mutant tumors (n=45) with *ARID1A* wild type (n=63) tumors (Supplementary Fig. 4A). *TRIM28* amplification and *CDK8* deletion were significantly retained only in *ARID1A* mutant tumors (p<0.0001 and p=0.0067, respectively), whereas *EGFR* amplification was significantly retained only in *ARID1A* wild type tumors (p=0.0054) (Supplementary Fig. 4B-C).

Integration of kinome mutations and CNA

Both kinome sequencing and SNP data were available for 106 tumors. After merging all mutations and CNA events in the PI3K/AKT/mTOR, MAPK and DNA repair pathway and ERBB family of receptor tyrosine kinases, we identified at least one event in 103 of 106 tumors analyzed (97%) (Fig. 3A).

Amplification incidence of >10% was found in the PI3K/AKT/mTOR-related genes *AKT2* (17%), *PIK3R2* (14.2%), *PIK3CA* (12.3%), *AKT1* (10.4%), the ERBB family of receptor tyrosine kinases *ERBB2* (19.8%) and *EGFR* (17%), and the DNA repair genes *PRKDC* (24%) and *CHEK2* (12.3%). *AKT2*, *PIK3R2*, *ERBB2*, *EGFR* and *CHEK2* primarily contained amplifications, from which only *ERBB2* (n=2) and *EGFR* (n=1) presented tumors that were both amplified and mutated. *PIK3CA* was mostly mutated, yet four *PIK3CA* mutant tumors carried both an amplification and a mutation. Amplifications and mutations

never co-occurred in *AKT1* and *PRKDC*.

Deletion incidence of >10% was observed in the PI3K/AKT/mTOR-related gene *PIK3C3* (18.9%) and the DNA repair genes *PALB2* (30.2%), *ATM* (17.9%) and *BRCA2* (17%). *PIK3C3*, *PALB2* and *BRCA2* primarily harbored deletions, while *ATM* deletions and mutations co-occurred in three tumors.

We hypothesized that the alterations in genes described in Figure 3A can be added up to promote aberrant pathway signaling. Mutations or CNA occurred in PI3K/AKT/mTOR in 84.9% of tumors, in MAPK pathway in 27.4% of tumors and in ERBB receptor family of kinases in 42.5% of tumors. Combined mutations and CNA in PI3K/AKT/mTOR and MAPK pathway genes and the ERBB family of receptor tyrosine kinases indicated that 91% of all tumors were affected (Fig. 3B), while the DNA repair pathway was affected in 82% of all tumors (Fig. 3C).

Kinome profile reveals tumor clusters with differential survival

Clinical data was available for a subset of patients (n=70) (Supplementary Table 4). Disease-specific survival analysis revealed that *ARID1A*, *PIK3CA* or *ARID1A* plus *PIK3CA* alterations were not related to survival (Supplementary Fig. 5A-C). Kinome mutations and CNA events of all 106 tumors were integrated, and the tumors were grouped using K-means consensus clustering. Maximum cluster number was set at 8, since more clusters only marginally decreased friction (Supplementary Fig. 5D-F). Most tumors grouped together in cluster 1 (n=53), 3 (n=27) or 5 (n=13). A trend for worse disease-specific survival was demonstrated
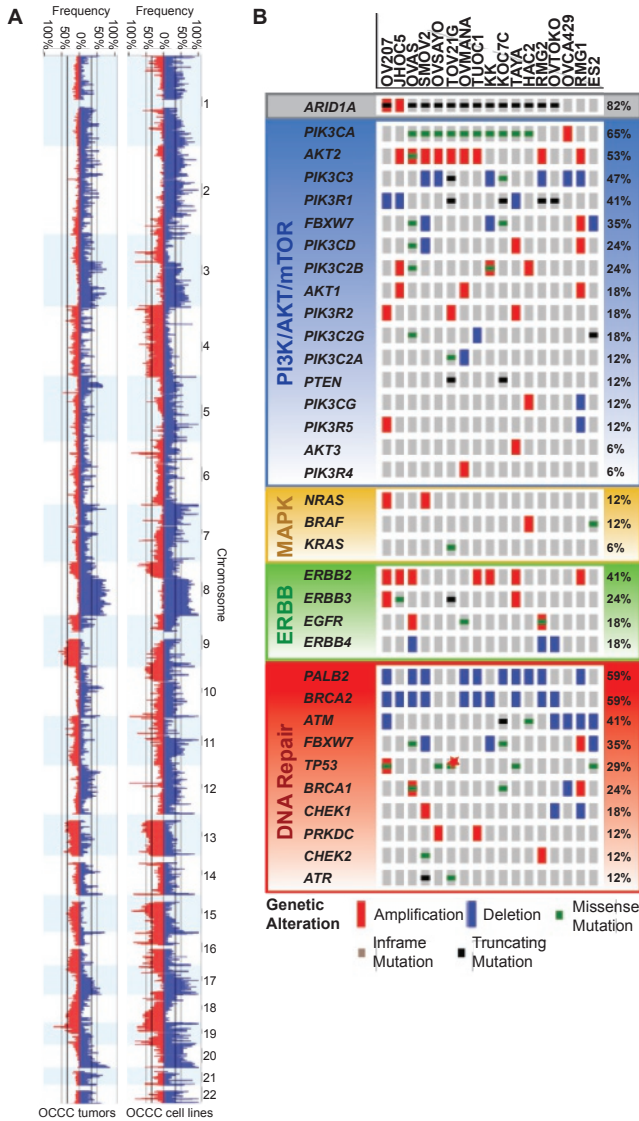
Figure 4 | OCCC cell line CNA and mutation distribution. (A) Chr 1-22 CNA (amplifications in blue, deletions in red) in OCCC tumors (n=108) and cell lines (n=17) depicted from Nexus Copy Number. **(B)** OCCC cell lines nonsynonymous mutation distribution in genes involved in the frequently mutated PI3K/AKT/mTOR (blue), MAPK pathway (yellow), ERBB family of receptor tyrosine kinases (green) and DNA repair (red) pathway as well as *ARID1A* and *PALB2* are shown with OncoPrint. CNA for each mutated gene are added. The 17 OCCC cell lines that were both kinome sequenced and SNP arrayed are shown on the horizontal axis ordered on total event frequency in the subsequently altered pathways. JHOC5 and OV207 are *ARID1A* mutant but retain ARID1A expression. The genes *AKT2*, *PIK3C3*, *PIK3CD*, *PIK3C2B*, *PIK3R2*, *PIK3C2G*, *PIK3C2A*, *PIK3CG*, *AKT3*, *PIK3R4*, *ERBB4*, *PALB2* and *CHEK1* were not sequenced in JHOC5, HAC2 and OVCA429, *TP53 mutation in TOV21G was detected just above threshold.

with cluster 3 compared with all other clusters (*p*=0.0638) (Supplementary Fig. 5G-H), which became highly significant upon selection for advanced stage OCCC patients (*p*<0.001, n=31) (Supplementary Fig. 5I). Grouping of mutation and CNA status for each cluster did not reveal unique genes in cluster 3 (Supplementary Fig. 5J-K).

Kinome profile based inhibitor screen identifies mTORC1/2 inhibition susceptibility

Kinome sequencing and SNP data of 17 OCCC cell lines presented similar alteration frequencies in PI3K/AKT/mTOR, MAPK and DNA repair pathway genes and the ERBB family of receptor tyrosine kinases as those observed in OCCC patients (Fig. 4A-B). However, an

A

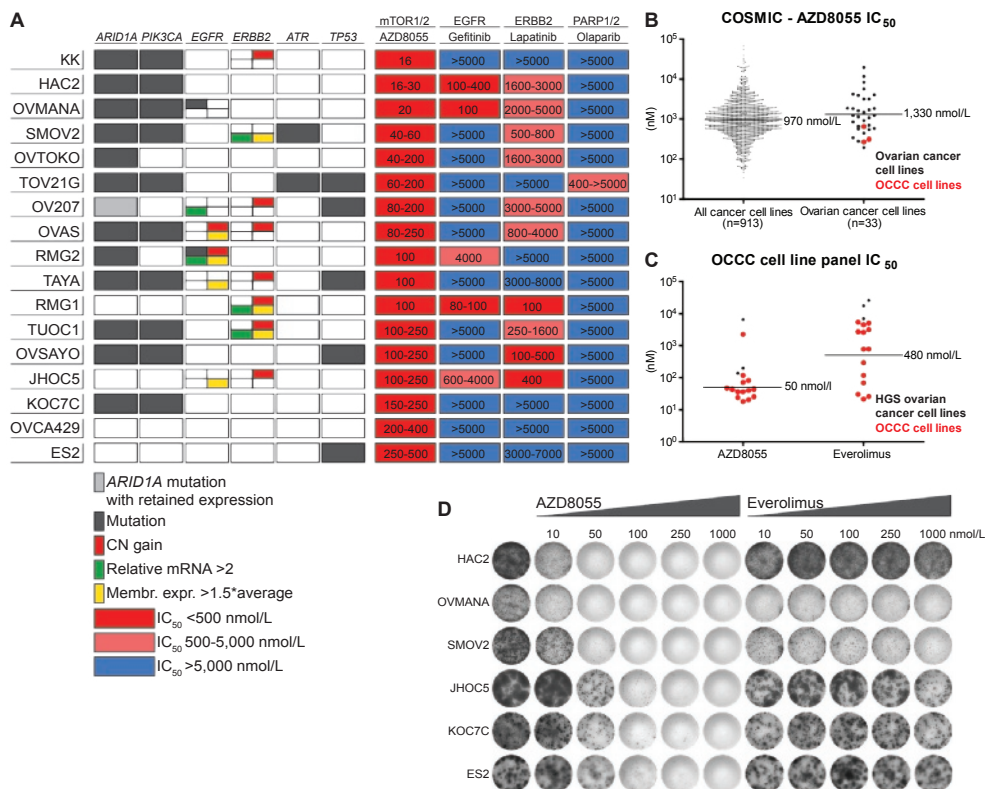|	ARID1A	PIK3CA	EGFR	ERBB2	ATR	TP53	mTOR1/2 AZD8055	EGFR Gefitinib	ERBB2 Lapatinib	PARP1/2 Olaparib
KK							16	>5000	>5000	>5000
HAC2							16-30	100-400	1600-3000	>5000
OVMANA							20	100	2000-5000	>5000
SMOV2							40-60	>5000	500-800	>5000
OVTOKO							40-200	>5000	1600-3000	>5000
TOV21G							60-200	>5000	>5000	400->5000
OV207							80-200	>5000	3000-5000	>5000
OVAS							80-250	>5000	800-4000	>5000
RMG2							100	4000	>5000	>5000
TAYA							100	>5000	3000-8000	>5000
RMG1							100	80-100	100	>5000
TUOC1							100-250	>5000	250-1600	>5000
OVSAYO							100-250	>5000	100-500	>5000
JHOC5							100-250	600-4000	400	>5000
KOC7C							150-250	>5000	>5000	>5000
OVCA429							200-400	>5000	>5000	>5000
ES2							250-500	>5000	3000-7000	>5000

Legend:
- *ARID1A* mutation with retained expression
- Mutation
- CN gain
- Relative mRNA >2
- Membr. expr. >1.5*average
- IC_{50} <500 nmol/L
- IC_{50} 500-5,000 nmol/L
- IC_{50} >5,000 nmol/L

B

COSMIC - AZD8055 IC_{50}

970 nmol/L — All cancer cell lines (n=913)
1,330 nmol/L — Ovarian cancer cell lines (n=33); OCCC cell lines

C

OCCC cell line panel IC_{50}

50 nmol/l — AZD8055
480 nmol/L — Everolimus
HGS ovarian cancer cell lines; OCCC cell lines

D

AZD8055 — 10, 50, 100, 250, 1000 nmol/L
Everolimus — 10, 50, 100, 250, 1000 nmol/L

HAC2, OVMANA, SMOV2, JHOC5, KOC7C, ES2

Figure 5 | OCCC cell line panel inhibitor screening. (A) Schematic representation of mutation status, mRNA level, copy number gain, membrane receptor expression and a heatmap of inhibitor IC_{50} in 17 OCCC cell lines. For each cell line horizontally: mutation status of the genes *ARID1A*, *PIK3CA*, *EGFR*, *ATR* and *TP53* are indicated in grey, *EGFR* and *ERBB2* mRNA level relative to GAPDH >2 are indicated in green, copy number gain is indicated in red and EGFR and ERBB2 membrane expression relative to average mean fluorescence intensity >2 are indicated in yellow. Cell line IC_{50} for AZD8055 (mTORC1/2), gefitinib (EGFR), lapatinib (ERBB2) and olaparib (PARP1/2) are shown horizontally, and cell lines are vertically ordered on AZD8055 sensitivity. **(B)** IC_{50} of the mTORC1/2 inhibitor AZD8055 from COSMICs (Cancerxgene.org) drug screening database for all cancer cell lines vs. ovarian cancer cell lines, horizontal lines indicate geometric mean. **(C)** AZD8055 and everolimus IC_{50} determined for 14 OCCC cell lines (ES2, KOC7C, SMOV2, JHOC5, RMG1, OVMANA, HAC2, OV207, OVTOKO, TOV21G, OVAS, OVCA429, TUOC1 and RMG2) by MTT assay. HGS ovarian cancer cell lines PEA1, PEO14 and OVCAR3 were used as a resistant controls. Horizontal lines indicate geometric mean of only the OCCC cell lines. Data is derived from n≥2 experiments. **(D)** Long-term proliferation assay after exposure to increasing concentrations of AZD8055 and everolimus. Results are representative of n=3 experiments.

overrepresentation of *ARID1A* and *TP53* mutations and an underrepresentation of *KRAS* mutations were found. Due to the resemblance of OCCC patient alterations with those in the cell line panel, we decided to screen for kinase inhibition vulnerabilities of the PI3K/AKT/mTOR and MAPK pathway downstream targets mTORC1/2 and the ERBB receptor tyrosine kinases EGFR and ERBB2. In addition, the DNA repair pathway was targeted. High-throughput drug sensitivity testing revealed nanomolar range efficacy against the mTORC1/2

inhibitor AZD8055 in all 17 OCCC cell lines tested (Fig. 5A). Sensitivity appeared to be irrespective of *PIK3CA* or *ARID1A* mutation status, suggesting that alterations upstream of mTORC1/2 may explain the comprehensive AZD8055 susceptibility. COSMICs cancer cell line drug screening data (n=913 cell lines) with AZD8055 (Cancerrxgene.org) and temsirolimus (targeting mTORC1) indicate that OCCC cell lines are among the most sensitive ovarian cancer cell lines (Fig. 5B and Supplementary Fig. 6A).

MTT assay-based IC_{50} determination in 14 out of 17 OCCC cell lines demonstrated higher susceptibility to AZD8055 and the mTORC1 inhibitor everolimus in comparison to three HGS ovarian cancer cell lines (Fig. 5C). In contrast to AZD8055, proliferation inhibition by everolimus displayed a plateau phase in a wide concentration range and a large variation in sensitivity among OCCC cell lines (Fig. 5D and Supplementary Fig. 6B). Moreover, everolimus treatment resulted in increased p-AKT[473] levels, while AZD8055 and MLN0128, another mTORC1/2 inhibitor, reduced this upregulation (Supplementary Fig. 6C). AZD8055 and dactolisib, an mTORC1/2-PI3K inhibitor for which OCCC cell lines are highly sensitive (Supplementary Fig. 6A), strongly reduced p-AKT[473] and to a lesser extent p-AKT[308] at high concentrations (Supplementary Fig. 6D). The absence of PARP cleavage indicated that everolimus, AZD8055 and dactolisib do not induce apoptosis in an in vitro setting (Supplementary Fig. 6D). OCCC cell lines presented a large IC_{50} variation for upstream inhibitors of the PI3K/AKT/mTOR and MAPK pathway, e.g. PI3K inhibitor GDC0941 and MEK inhibitor selumetinib, compared with AZD8055 and dactolisib (Supplementary Fig. 6E). Long-term proliferation inhibition by dactolisib was stronger compared with AZD8055 (Supplementary Fig.

6F). Limited sensitivity was observed towards the EGFR inhibitor gefitinib and ERBB2/EGFR inhibitor lapatinib. *EGFR* mutations were observed in two cell lines, but only OVMANA (R705K) displayed gefitinib sensitivity. In cells with elevated levels of *ERBB2* mRNA and high ERBB2 membrane expression (RMG1, SMOV2 and TUOC1), lapatinib sensitivity was observed (Fig. 5A). However, some of the tested cell lines without *EGFR* mutations or elevated ERBB2 levels also displayed sensitivity to gefitinib and lapatinib, indicating involvement of alternative mechanisms. The PARP1 inhibitor olaparib showed some efficacy against *ATR* mutant TOV21G cells.

In conclusion, OCCC cell lines exhibit exquisite sensitivity to mTORC1/2 inhibitors, whereas limited sensitivity was observed towards ERBB receptor tyrosine kinase and DNA repair inhibitors despite the high aberration frequency in those pathways.

Targeting of mTORC1/2 is effective in PDX models

Considering the high susceptibility of OCCC cell lines to AZD8055, we validated mTORC1/2 activity in OCCC tumor samples. Immunostaining of the mTORC1/2 downstream target p-S6 was performed on two different tissue microarrays (n=136 and n=83) with primary tumor material from HGS ovarian cancer and OCCC. OCCC tumors were more frequently p-S6 positive compared to HGS ovarian cancer in both datasets (*p*=0.053 and *p*=0.0028, respectively) (Fig. 6A-C). Subsequently, we tested AZD8055 efficacy in OCCC PDX-bearing NSG mice. Sequencing of 19 genes with the highest mutation frequency in OCCC patients showed mutations in *ARID1A* (1148* stop-gain), *PTEN* (H93R) and *BRCA1* (V356A and 1533* stop-gain) in PDX.155, in *PIK3CA* (K111E, recurrent in OCCC tumors) and *ATM* (T1020I) in PDX.180 and none in
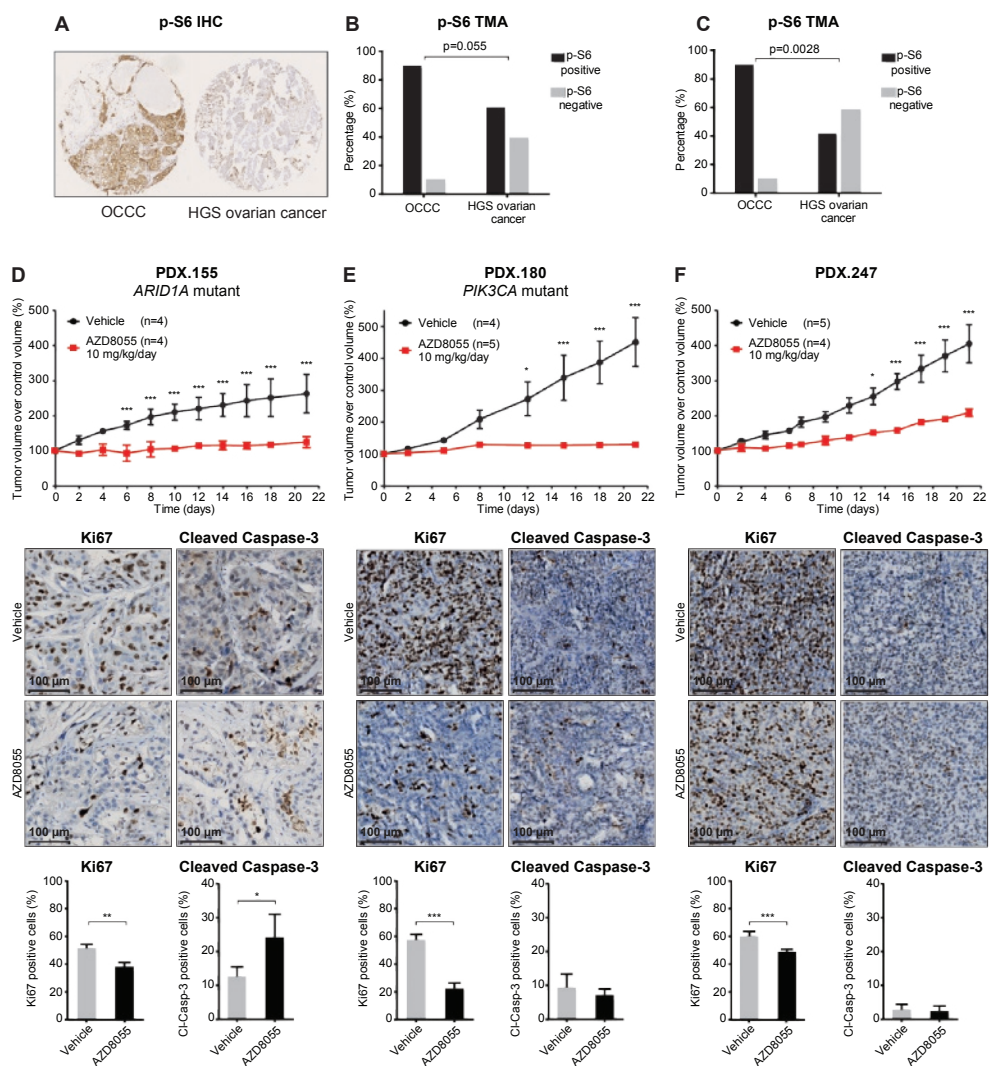
Figure 6 | p-S6 expression and mTORC1/2 inhibition in OCCC PDX models. (A) Representation of p-S6 expression in an OCCC tumor (left) and HGS ovarian cancer tumor (right) as determined by IHC on TMA. **(B)** Percentage of positive p-S6 expression in primary OCCC tumors (positive n=10, negative n=1) and HGS ovarian cancer tumors (positive n=76, negative n=49), **(C)** and positive p-S6 expression in a second TMA of primary OCCC (positive n=10, negative n=1) and HGS ovarian cancer tumors (positive n=30, negative n=42), determined by Fisher's exact test, two-tailed. **(D)** Tumor growth, Ki67 expression and Cleaved Caspase-3 positivity in PDX.155, **(E)** PDX.180 and **(F)** PDX.247 tumors following AZD8055 or vehicle treatment. PDX.155 vehicle mice were treated in F4 generation and AZD8055 mice were treated in F5 generation. Tumor volume is represented as percentage of initial tumor volume at start of treatment. Quantification of Ki67 and Cleaved Caspase-3 positivity in tumors from vehicle and AZD8055 treated mice, sacrificed on day 21, are shown below respective PDX model tumor growth charts. * indicates $p<0.05$, ** indicates $p<0.01$ and *** indicates $p<0.001$.

PDX.247. All mutations were present in the sequenced F0 (patient tumor), F1 and F2 generation. GISTIC analysis indicated CNA across the PDX models that resemble CNA in OCCC patients (Supplementary Fig. 7A). Significant growth differences were observed between AZD8055 (10 mg/kg/day) and vehicle-treated mice in all three PDX models (Fig. 6D-F). AZD8055 treatment reduced tumor growth in PDX.247 and inhibited tumor growth in PDX.155 and PDX.180, which is reflected in a reduction of proliferation marker Ki67 positivity (Fig. 6D-F). Remarkably, an increased staining of the apoptosis marker Cleaved Caspase-3 was observed in PDX.155 after AZD8055 treatment (Fig. 6D-F). Phosphorylation of mTORC1/2 downstream target S6 was clearly detectable in the vehicle treated tumors but did not significantly change after AZD8055 treatment (Supplementary Fig. 7B-D).

DISCUSSION

Advanced stage OCCC patients respond poorly to standard platinum-based chemotherapy, indicating an unmet need for novel treatment strategies. Kinome sequencing of 518 kinases and 79 cancer-related genes and SNP array analysis of 108 OCCC tumors revealed mutations, amplifications and deletions in well-known genes such as *ARID1A*, *PIK3CA*, *TP53* and *KRAS* and several newly identified genes. Collectively, alterations in genes from the PI3K/AKT/mTOR pathway, the MAPK pathway and the ERBB family of receptor tyrosine kinases were found in 91% of tumors. In line with these alterations, high mTOR signaling was frequently observed in OCCC and mTORC1/2 inhibition was highly effective in OCCC cell lines and PDX models. These results indicate that especially targeting mTOR1/2 could be an effective therapeutic approach for OCCC patients.

ARID1A was the most common mutated gene in our OCCC dataset, with a mutation rate of 46.6%. Overall, the mutation rates observed for *ARID1A*, *PIK3CA*, *TP53* and *KRAS* matched earlier sequencing studies on smaller OCCC datasets (3, 4, 6, 8, 9, 24). Moreover, mutation incidences in *PIK3CA*, *TP53* and *KRAS* correlated with the frequencies found in 'pure OCCC' tumors as described by Friedlander *et al*. (22), indicating that our sample cohort also contains pure OCCC tumors. *ARID1A* and *PIK3CA* mutations have been shown as early onset mutations in the development of OCCC (23, 25). Previous studies have shown that onset of oncogenesis regularly requires two or more mutational hits in a proto-oncogene or tumor suppressor gene, as was demonstrated in a de novo OCCC mouse model (26). Indeed, in our tumor cohort, 94% of the *PIK3CA* and *ARID1A* mutant tumors contained at least one additional mutation or CNA in PI3K/AKT/mTOR, MAPK or DNA repair pathway genes or the ERBB family of receptor tyrosine kinases, which was stage independent. Considering earlier reports and our observed OCCC mutation pattern, we hypothesize that a mutation in *ARID1A* or *PIK3CA* is accompanied by either a CNA or mutation in one of the aforementioned pathways to promote onset of OCCC. A limitation of the present study can be the imbalance in tumor samples and matched controls. Accordingly, we could designate a restricted number of mutations as somatic. Not all clinical data were available and therefore we may have underestimated the relation between kinome alteration status and clinicopathological characteristics or clinical outcome.

Genes mutated at low frequency (1-10%) are generally difficult to designate as oncogenic drivers. Therefore, we used a large OCCC dataset and binomial testing of observed kinome variants. Eleven genes were found to

be significantly mutated relative to the background mutation rate, and some of these had not previously been described in OCCC. Validation of variants in these low-mutation-frequency genes across multiple cancer types using the COSMIC database enabled us to predict *AKT1*, *PIK3R1*, *FBXW7*, *ERBB3*, *ATM*, *CHEK2* and *MYO3A* as novel drivers of OCCC (27). Functional effects of *AKT1* and *PIK3R1* mutations in these domains were described in previous research. For instance, mutations in the *AKT1* PH-domain were shown to constitutively activate AKT1 (18). Likewise, mutations in the *PIK3R1* inter SH1-SH2 domain resulted in loss of PIK3R1 function, thus generating PIK3CA hyperactivation (19). These studies support the assumption that *AKT1* and *PIK3R1* are oncogenic drivers in OCCC. Furthermore, *AKT1*, *PIK3R1*, *FBXW7* and *ERBB3* all contribute to mTOR signaling, while *ATM*, *CHEK2* and *FBXW7* are implicated in DNA repair signaling (19, 21, 28). *MYO3A* mutations are found infrequently in cancer, but are still implicated in resistance to trastuzumab in breast cancer (29).

In the present study, kinome sequencing and SNP array analysis revealed substantial percentages of *EGFR* and *ERBB2* mutations or amplifications in OCCC tumors. *EGFR* amplifications (associated with endometriosis, a precursor of OCCC) and *ERBB2* amplifications were previously demonstrated in OCCC by comparative genomic hybridization (30, 31). Furthermore, sensitivity towards the clinically available inhibitors gefitinib and lapatinib was shown in OCCC cell lines harboring *EGFR* or *ERBB2* alterations and may be explored further in the clinic (32, 33). In previous studies, EGFR-targeting therapy such as gefitinib or erlotinib and EGFR-ERBB2 targeting therapy using lapatinib did not provide clinical benefit in pretreated ovarian cancer patients (34-36), but these studies did not focus on OCCC patients. Additionally, alterations in DNA repair pathway genes were identified in 82% of tumors, suggesting opportunities to target DNA repair cascades in OCCC in future research. Unfortunately, PARP1/2 inhibition by olaparib was not effective in our OCCC cell line panel, including *BRCA1* mutant cell lines. Interestingly, inhibition of PARP1/2 by the PARP trapping agent talazoparib demonstrated efficacy in a subset of OCCC cell lines (37).

Mutations in *mTOR* have been detected in several tumor types including HGS ovarian cancer (38). Although *mTOR* mutations were not found in OCCC tumors, alterations in upstream pathways that promote mTORC1/2 activation were found in 91% of these tumors. In line with these results, abundant high p-S6 expression was observed in OCCC tumors compared to HGS ovarian cancer tumors. Moreover, OCCC cell lines demonstrated nanomolar range sensitivity towards the mTORC1/2 inhibitor AZD8055 and higher sensitivity compared with HGS ovarian cancer cell lines. To our knowledge we were the first to exploit the use of PDX models of OCCC. In vivo administration of AZD8055 resulted in a significant growth inhibitory effect in three OCCC PDX models, consisting of a *PIK3CA* mutant, an *ARID1A* mutant and a *PIK3CA* and *ARID1A* wild type model. These models reflect the genetic makeup of OCCC. Hence, we propose mTORC1/2 inhibition as a future treatment strategy in OCCC that should be explored with urgency. Additional inhibition of *ARID1A* synthetic lethal targets in combination with mTORC1/2 inhibition can be utilized in *ARID1A* mutant OCCC tumors (14, 15).

In the clinic, inhibition of mTORC1 with temsirolimus added to standard chemotherapy did not improve overall survival in newly diagnosed stage 3-4 OCCC patients as compared to historical

controls (39). However, by blocking both mTORC1 and mTORC2, re-activation of PI3K and MAPK signaling via mTORC2 can be prevented in OCCC. This may contribute to a better response in OCCC patients. AZD8055 and another mTORC1/2 inhibitor, OSI-027, were tested in non-OCCC cancer types. Disappointingly, anti-tumor efficacy was only observed above maximum tolerated dose and both drugs are no longer in clinical development (40, 41). Based on our results, it is conceivable that tumor responses in OCCC patients can be attained at or below maximum tolerated dose with AZD8055 or OSI-027. A new generation of mTORC1/2 inhibitors, such as MLN0128 (sapanisertib), is now being evaluated in multiple phase II clinical trials (NCT02724020 and NCT02725268). Given the large variation in mutations in specific genes of the PI3K/AKT/mTOR and MAPK pathway between patients and the high variation in sensitivity towards PI3K and MEK inhibition in our OCCC cell lines, PI3K or MEK monotherapy tumor responses in OCCC patients will presumably be limited. MLN0128 is now being combined with a PI3Kα inhibitor (MLN1117) in an ongoing phase II trial in advanced endometrial cancer (NCT02725268). Drugs targeting PI3K as well as mTORC1/2, e.g. dactolisib, DS-7423 and XL765, showed high toxicity in the clinical setting, despite promising efficacy in in vitro cancer models, including OCCC (16, 42-45). Based on our mutational analysis in OCCC patients, drug sensitivity screens and molecular analyses in OCCC cell lines, a strategy that combines inhibition of mTORC1/2 with PI3K or MEK will have the highest likelihood to improve clinical benefit for the majority of OCCC patients. However, the use of single target inhibitors of mTORC1/2, PI3K and MEK at suboptimal concentrations is probably crucial to maximize efficacy and minimize toxicities that were observed with PI3K-mTORC1/2 dual inhibitors.

Overall, our findings set the stage to explore mTORC1/2 targeting phase II clinical trials in OCCC in the future.

MATERIAL AND METHODS

Sample collection
Primary tumor samples from 124 OCCC patients and 47 paired control blood samples were prospectively collected from Belgium, Germany, Norway, Poland, the Netherlands, UK and USA. All patients gave written informed consent for samples to be collected and the corresponding ethical review boards approved the study. Tumor samples had to contain ≥40% tumor cells, of which ≥70% was OCCC, as determined by experienced gynecologic oncology pathologists. We obtained 17 human OCCC cell lines: TOV21G (ATCC, USA); RMG1, RMG2, OVMANA, OVTOKO and HAC2 (JCRB Cell Bank, Japan); JHOC5 (RIKEN Cell Bank, Japan); OVCA429 (Cell Biolabs, USA); OVSAYO, TUOC1, KK, OVAS, SMOV2 and KOC7C (Dr. Hiroaki Itamochi, Tottori University School of Medicine, Tottori, Japan); ES2 (Dr. Els Berns, Erasmus MC, Rotterdam, The Netherlands); TAYA (Dr. Yasushi Saga, Jichi Medical University, Yakushiji, Shimotsuke-shi, Tochigi, Japan) and OV207 (Dr. Vijayalakshmi Shridhar, Mayo Clinic, Rochester, MN, USA). All cell lines were maintained in RPMI supplemented with 10% FCS, 100 µg/ml Penicilin/Streptomycin and 2 mM L-Glutamine. All cell lines were tested by STR profiling and were mycoplasma free. All cell lines were kept in culture for a maximum of 50 passages.

Kinome sequencing
Library construction, exome capture and sequencing: From 124 primary fresh frozen OCCC tumors and 47 paired controls, 3 µg DNA was prepared for sequencing using the following steps. Genomic DNA was sheared to produce 300 bp fragments (Covaris

4

S220 USA); using *SureSelect Target enrichment & Human Kinome Kit* (Agilent technologies®, USA) kinase exons were tagged and captured; using biotinylated RNA library baits and streptavidin beads, exons were amplified and loaded on a HiSeq2500 Illumina sequencer using paired-end sequencing according to manufacturer's protocols. The *SureSelect Human Kinome Kit* captures exons from 518 kinases, 13 diglyceride kinases, 18 PI3K domain and regulatory component genes and 48 cancer related genes (Supplementary Table 1, available online). After sequencing, raw data was mapped to the human reference sequence NCBI build 37 (hg19) and processed according to our sequencing pipeline (Supplementary Fig. 1). Genome Analysis Toolkit (GATK, version 1.0.5069) was used for indel re-alignment and base quality recalibration on BAM files.

Genotype calling and quality control: Using the *SAMtools-mpileup* algorithm, genotype calling on identified variants was performed. BAM alignment files from all samples were combined and only variants of high quality were retained. Quality thresholds were the following: a minimum mapping quality of 40 reads, minimum coverage of 10 reads and a minimum variant-containing read fraction of 0.1 with a minimum coverage of 5 reads.

Variant filtering and prediction of functional significance of missense mutations: Only variants with a high probability of having an effect on protein function were retained (according to Ensembl variation prediction). These variants included splice donor variant, splice acceptor variant, stop-gain, frameshift variant, initiator codon variant, inframe insertion, inframe deletion, missense variant. Missense variant functional effects were predicted in silico with PolyPhen-2 (prediction based on amino acid (aa) structure) and SIFT (prediction based on degree of aa conservation) mutation assessor algorithms (46, 47). For 47 out of 124 tumors we acquired paired control samples to exclude germline variants. Identified novel mutations in the 47 tumors with paired control were classified as somatic. Characterized novel mutations in tumors without paired control were classified as candidate somatic. Subsequently, population single nucleotide polymorphisms variations present in the exome variant server were excluded, and variants found in the genes *MIR548N*, *TTN* and *OBSCN* were removed for further analysis. Mutated genes with a >4% mutation incidence across the OCCC tumors and genes depicted in OncoPrinter figures were manually assessed in Intergrative Genomics Viewer© (IGV) (48). Only variants present in IGV were retained for further analysis. Our variant filtering pipeline is summarized in Supplementary Figure 1.

Haloplex sequencing: We sequenced 40 genes, including 19 high mutation frequency genes (genes mutated in >4% of OCCC tumors), *ARID1A* and other cancer-related genes were sequenced using the same OCCC tumor samples for re-validation of the mutations using Haloplex custom kit, (Agilent technologies®, USA) (Supplementary Table 2). In nine out of 124 tumor samples the DNA quantity was too low to perform sequencing. Five additional paired control samples were included in this sequencing step, which revealed a total of four germ line variants: *ATR* (n=2), *TRRAP* (n=1) and *MYO3A* (n=1). Only variants present in IGV were retained for further analysis. Haloplex sequencing revealed four variants (*ATM*, *ERBB3*, *PTEN*, *PIK3R1*, one variant in each gene) also present in kinome sequencing, but below the read coverage thresholds.

SNP array
SNP genotyping, quality control: Genome-

wide SNP genotyping was performed with *HumanOmniExpressExome-8BeadChip* (Illumina, USA) containing >900K SNPs, including >273K functional exomic markers to determine CNA in 108 primary OCCC tumors and 17 OCCC cell lines. DNA sample processing, hybridization, labeling, scanning and data extraction was performed according to Illumina infinium 2 protocol. Illumina GenomeStudio software was used for primary sample assessment and SNP call rate quality control of SNP intensity output files.

Normalization and analysis: SNP names, sample IDs, chromosome, position and raw X and Y SNP probe intensity data were exported from GenomeStudio software. Raw X and Y SNP probe intensity were normalized using GenomeStudio and subsequently corrected for non-genetic factors caused by dye bias and probe specific noise using principal components analysis. These methods were described previously (49). Next, the ratio of filtered SNP probe intensities was determined by comparing with SNP probe intensities in a control sample dataset (n=1536, 731 male and 756 female, kindly provided by Dr. GH Koppelman, Pediatric Pulmonology and Pediatric Allergology, Beatrix Children's Hospital, University Medical Center Groningen, the Netherlands) SNP genotyped using *HumanOmniExpressExome-8BeadChip* on the same Illumina BeadArray reader. In this way array-reader-specific bias and signals of normal individuals were excluded. SNP probe intensities were converted to log-R-ratios and CNA were determined by a circular binary segmentation algorithm in the DNA copy module (version 1.40.0), conducted in R (50, 51). To determine significant CNA, the segmented copy numbers were analyzed with GISTIC version 2.6.2 on the Genepattern server from the Broad Institute, USA) (52). Parameters used for running GISTIC included the following:

refgene file Hg 19, amplification threshold: 0.3, deletion threshold: -0.3, join segment size: 6, Q threshold: 0.05, remove X: yes. Other parameters were used under default settings. GISTIC was used to identify CNA that were over-represented in our dataset based on frequency and amplitude of each alteration, defined by a G-score. Subsequently, a p-value was assigned to each G-score based on background G-score distribution corrected by false discovery rate statistics. We used high-level amplification (LogR ratio above 0.3) and deletion (LogR ratio below -0.3) thresholds to identify focal gains and losses above the levels observed in whole chromosome arms, as described by The Cancer Genome Atlas (1, 53).

K-means consensus clustering of kinome mutations and CNA

For unsupervised identification of tumors with similar CNA and mutation profiles, we used the "ConsensusClusterPlus" package 3.3 (54). CNA and mutation data per kinase were integrated for each tumor according to the following criteria: amplification + activating mutation = 3, activating mutation = 2, amplification = 1, no alteration/amplification + deleterious mutations/deletion + activating mutation = 0, deletion = -1, deleterious mutation = -2, deletion + deleterious mutation = -3. We used a data matrix of the aforementioned values and standard parameters using euclidean distance, up to k=10 groups, and n=1000 bootstrapped sampling with 80% resampling in each iteration. Used kinase CNA were extracted directly from GISTIC analysis, and kinase mutations were evaluated for activating or deactivating effects on protein function using SIFT and PolyPhen-2 predictor algorithms.

mRNA level determination

The 7500 Fast Real-Time PCR System from Applied Biosystems was used to measure mRNA levels that were

normalized to expression of *GAPDH*. The following primer sequences were used in the SYBR® Green master mix (Roche, Switzerland): *GAPDH*_Forward, AAGGTGAAGGTCGGAGTCAA; *GAPDH*_Reverse, AATGAAGGGGTCATTGATGG; *ERBB2*_Forward, AGCATGTCCAGGTGGGTCT; *ERBB2*_Reverse, CTCCTCCTCGCCCTCTTG ; *EGFR*_Forward, TCCTCTGGAGGCTGAGAAAA; *EGFR*_Reverse, GGGCTCTGGAGGAAAAGAAA.

Flow cytometry
Cells were stained with cetuximab antibody (Merck KGaA, Germany) or trastuzumab antibody (Roche, Switzerland) and subsequently stained with FITC conjugated monoclonal mouse anti-human secondary antibody (Sigma-Aldrich, USA). At least 10.000 events were measured on a FACS Calibur (Becton Dickinson, USA). FlowJo software was used for data analysis. Mean fluorescence intensity of >two * average fluorescence intensity among all measured OCCC cell lines was defined as overexpression.

MTT assays
Cells from the afore mentioned OCCC cell lines and the HGS ovarian cancer cell lines PEA1, PEO14 and OVCAR3 were plated in 96-wells plates and incubated overnight before 96-hour treatment with increasing concentrations of AZD8055, GDC0941, selumetinib, dactolisib (Axon Medchem, the Netherlands) or everolimus (Santa Cruz, USA). After 96 hours MTT was added to a final concentration of 0.5 mg/ml and cells were incubated for 4 additional hours. Cells were then dissolved in DMSO, and the produced formazan was measured at 520 nm with a Bio-Rad iMark spectrometer.

Long-term proliferation assays
Cells were seeded in 12-well plates and incubated overnight before everolimus, AZD8055 or dactolisib was added. After 10-13 days cells were fixed with 4% formaldehyde, stained with 0.1% crystal violet and subsequently the plates were scanned. Plating concentrations were; OVMANA 8000 cells/well, HAC2 5000 cells/well, SMOV2 5000 cells/well, JHOC5 1000 cells/well, ES2 500 cells/well and KOC7C 250 cells/well.

Western blotting
For western blotting primary antibodies against p-AKT[308] (9275), p-AKT[473] (9271), p-S6 (2211) and PARP (9532) were obtained from Cell Signaling Technology, USA. B-Actin (C4) was obtained from MPbiomedicals, USA. MLN0128 was obtained from Axon Medchem, The Netherlands.

In vitro inhibitor screening
The 17 OCCC cell lines were plated in 384 well plates with 250-2000 cells/well using an automatic cell dispenser. Cell lines were incubated with varying concentrations of AZD8055 (Axon Medchem, The Netherlands), gefitinib (Selleckchem, USA), lapatinib (Selleckchem, USA) or olaparib (Axon Medchem, The Netherlands) for six days. Cell viability was subsequently monitored using CellTiter-Blue cell viability assay (Promega, USA). Due to large cell density dependent variability in drug sensitivity, for each cell line the lowest and highest IC_{50} were removed. The cell lines CAPAN1, OE19, LOVO, OVCAR3, OVCAR4 and SKOV3 were exposed to AZD8055 to serve as sensitive and resistant controls.

AZD8055 in vivo administration
All animal experiments were approved by the Institutional Animal Care and Use Committee of the University of Groningen (Groningen, the Netherlands) and carried out in accordance with the approved guideline "code of practice: animal experiments in cancer research" (Netherlands Inspectorate for Health

Protection, Commodities and Veterinary Public Health, 1999).

Before surgery, all patients from whom tumor samples were obtained for PDX modeling gave written informed consent. PDX.155 was obtained from a FIGO stage IIIC OCCC patient, with no response to carboplatin/paclitaxel chemotherapy and 9 months disease-specific survival. PDX.180 was derived from a FIGO stage IIIC OCCC patient treated with neoadjuvant carboplatin/paclitaxel chemotherapy and 10 months disease-specific survival. PDX.247 was obtained from a FIGO stage IIB OCCC patient, treated with complete debulking surgery followed by carboplatin/paclitaxel chemotherapy and no evidence of disease after 24 months of follow-up. Surgical tissues were implanted and propagated successfully to the F3 or F4 generation according to previously described methods (55). PDX models were Haloplex sequenced as described above. F3 or F4 tumor pieces were cut into 3x3x3 mm3 sections and subcutaneously implanted in the flank of 12 to 16 week old NOD.CB17-Prkdcscid/NCrHsd (NSG) mice (internal breed, Central Animal Facility, University Medical Centre Groningen). Tumor growth was quantified at least once per 3 days by caliper measurements according to the formula (width^2 x length)/2. When tumors demonstrated sustained growth (on average after 27 days), mice were randomized into vehicle control or treatment groups (n=5 mice/group). AZD8055 (Axon Medchem, the Netherlands) (10 mg/kg in 10% DMSO, 40% Polyethylene glycol 300) or the vehicle were administered intraperitoneally daily. Treatment with AZD8055 or the vehicle was continued for 21 days, after which all mice were sacrificed. One mouse in the AZD8055 treated group died on treatment day nine due to undefined reasons. Tumor growth was determined by tumor volume/control tumor volume. For future analysis the tumors were resected and snap frozen at -80°C as well as paraffin embedded.

Immunohistochemical analysis

From paraffin-embedded PDX tumors and two TMAs containing 11 OCCC tumors and 125 HGS ovarian cancer tumors (56) and 11 OCCC tumors and 72 HGS ovarian cancers (57), slices (3 µm thick) were cut using a microtome and placed on 3-aminopropyltriethoxysilane-coated glass slides. Heat-induced antigen retrieval was performed in 10 mM citrate buffer using a 400 W rotary microwave. Endogenous peroxidase was blocked by 30 minutes incubation with 0.3% H_2O_2 in PBS. Endogenous avidin/biotin activity was blocked using a commercially available blocking kit (Vector Laboratories, USA). Slides were incubated with primary antibodies detecting human Ki67 (DAKO M7240, USA), Cleaved Caspase-3 (Cell Signaling #9661) and p-S6 (Cell Signaling #2211, USA). Staining was visualized after incubation with biotinylated or peroxidase-bound secondary antibodies (Dako, USA) using streptavidin-biotin/horseradish peroxidase complex (Dako, USA) and 3,3'-diaminobenzidine (Sigma-Aldrich, USA). Hematoxylin counterstaining was applied routinely, and hematoxylin & eosin (H&E) staining was used to analyze tissue viability and morphology. Photographs were acquired by digitalized scanning of slides using the NanoZoomer 2.0-HT multi-slide scanner (Hamamatsu, Japan). The PDX tumor stainings were quantified by scoring positive nuclei (Ki67) or positive cytoplasm (Cleaved Caspase-3) in five randomly assigned 40x magnified areas from each slide. The TMAs were scored in a semi-quantitative fashion incorporating both the intensity and distribution of the staining. The percentage of positive cells was categorized as absent (0-5%, 0), low (5-25% positive cells, 1), low-moderate (25-50% positive cells, 2), moderate-high (50-75% positive cells,

4

3) or high (75-100%, 4). The intensity of cytoplasmic staining was categorized as absent (0), weak (1), moderate (2) or strong (3). The intensity and proportion scores were then multiplied to give the weighted h-score.

Data visualization
For representation of data in figures and illustrations the following software tools were used; Adobe® Illustrator® CS6, Graphpad Prism® 6.01, BioVenn (58), cBioPortal OncoPrinter version 1.6.1 and R.

Statistical analysis
All filtered kinome sequencing variants were tested for binomial statistical significance at univariate level after multiple testing corrections using R. Clinical data (n=70) was imported in Graphpad Prism® 6.01. Disease-specific survival analysis was performed using the Kaplan-Meier method with Log-rank test to search for differences between groups, with $p<0.05$ as cutoff. Statistical significance for tumor growth was determined using 2-way ANOVA with Bonferoni post-hoc test correction. Statistical significance of immunohistochemical analysis was determined using a two-tailed Student's t-test. Statistical significance of mutual exclusivities between mutated genes were calculated using Fisher's exact test, two-tailed in Graphpad Prism® 6.01.

AUTHOR CONTRIBUTIONS

G.B.A.W., R.B., A.G.J.Z. and S.J. conceived and supervised the project. J.J.C. and K.B. performed the majority of experiments and data analysis with the assistance of G.B.A.W., R.S.N.F., T.T., H.K., G.J.M., E.M.H., A.M.C.G., E.W.D., D.W., R.J.C.K., and L.M.; H.I., A.K.L.R., M.J.B., H.B.S., I.G., E.N., J.B., E.I.B., J.K. and B.S. provided samples. J.J.C., G.B.A.W., A.G.J.Z and S.J. wrote the manuscript. All authors discussed the results and commented on the manuscript.

REFERENCES

1. Cancer Genome Atlas Research Network. Integrated genomic analyses of ovarian carcinoma. Nature. 2011 Jun 29;474(7353):609-15.
2. Anglesio MS, Carey MS, Kobel M, Mackay H, Huntsman DG, Vancouver Ovarian Clear Cell Symposium Speakers. Clear cell carcinoma of the ovary: a report from the first Ovarian Clear Cell Symposium, June 24th, 2010. Gynecol Oncol. 2011 May 1;121(2):407-15.
3. Wiegand KC, Shah SP, Al-Agha OM, Zhao Y, Tse K, Zeng T, et al. ARID1A mutations in endometriosis-associated ovarian carcinomas. N Engl J Med. 2010 Oct 14;363(16):1532-43.
4. Jones S, Wang TL, Shih I, Mao TL, Nakayama K, Roden R, et al. Frequent mutations of chromatin remodeling gene ARID1A in ovarian clear cell carcinoma. Science. 2010 Oct 8;330(6001):228-31.

5. Guan B, Wang TL, Shih I. ARID1A, a factor that promotes formation of SWI/SNF-mediated chromatin remodeling, is a tumor suppressor in gynecologic cancers. Cancer Res. 2011 Nov 1;71(21):6718-27.
6. Kuo KT, Mao TL, Jones S, Veras E, Ayhan A, Wang TL, et al. Frequent activating mutations of PIK3CA in ovarian clear cell carcinoma. Am J Pathol. 2009 May;174(5):1597-601.
7. Hashiguchi Y, Tsuda H, Inoue T, Berkowitz RS, Mok SC. PTEN expression in clear cell adenocarcinoma of the ovary. Gynecol Oncol. 2006 Apr;101(1):71-5.
8. Zannoni GF, Improta G, Chiarello G, Pettinato A, Petrillo M, Scollo P, et al. Mutational status of KRAS, NRAS, and BRAF in primary clear cell ovarian carcinoma. Virchows Arch. 2014 Aug;465(2):193-8.
9. Ho ES, Lai CR, Hsieh YT, Chen JT, Lin AJ, Hung MH, et al. P53 Mutation is Infrequent in Clear Cell Carcinoma of the Ovary. Gynecol Oncol. 2001 Feb;80(2):189-93.
10. Kuo KT, Mao TL, Chen X, Feng Y, Nakayama K, Wang Y, et al. DNA copy numbers profiles in affinity-purified ovarian clear cell carcinoma. Clin Cancer Res. 2010 Apr 1;16(7):1997-2008.
11. Rahman MT, Nakayama K, Rahman M, Katagiri H, Katagiri A, Ishibashi T, et al. Gene amplification of ZNF217 located at chr20q13.2 is associated with lymph node metastasis in ovarian clear cell carcinoma. Anticancer Res. 2012 Aug;32(8):3091-5.
12. Yamashita Y, Akatsuka S, Shinjo K, Yatabe Y, Kobayashi H, Seko H, et al. Met is the most frequently amplified gene in endometriosis-associated ovarian clear cell adenocarcinoma and correlates with worsened prognosis. PLoS One. 2013;8(3):e57724.
13. Helming KC, Wang X, Wilson BG, Vazquez F, Haswell JR, Manchester HE, et al. ARID1B is a specific vulnerability in ARID1A-mutant cancers. Nat Med. 2014 Mar;20(3):251-4.
14. Bitler BG, Aird KM, Garipov A, Li H, Amatangelo M, Kossenkov AV, et al. Synthetic lethality by targeting EZH2 methyltransferase activity in ARID1A-mutated cancers. Nat Med. 2015 Feb 16.
15. Bitler BG, Wu S, Park PH, Hai Y, Aird KM, Wang Y, et al. ARID1A-mutated ovarian cancers depend on HDAC6 activity. Nat Cell Biol. 2017 Aug;19(8):962-73.
16. Oishi T, Itamochi H, Kudoh A, Nonaka M, Kato M, Nishimura M, et al. The PI3K/mTOR dual inhibitor NVP-BEZ235 reduces the growth of ovarian clear cell carcinoma. Oncol Rep. 2014 Aug;32(2):553-8.
17. Sasano T, Mabuchi S, Kuroda H, Kawano M, Matsumoto Y, Takahashi R, et al. Preclinical Efficacy for AKT Targeting in Clear Cell Carcinoma of the Ovary. Mol Cancer Res. 2014 Dec 17.
18. Parikh C, Janakiraman V, Wu WI, Foo CK, Kljavin NM, Chaudhuri S, et al. Disruption of PH-kinase domain interactions leads to oncogenic activation of AKT in human cancers. Proc Natl Acad Sci U S A. 2012 Nov 20;109(47):19368-73.
19. Thorpe LM, Yuzugullu H, Zhao JJ. PI3K in cancer: divergent roles of isoforms, modes of activation and therapeutic targeting. Nat Rev Cancer. 2015 Jan;15(1):7-24.
20. Jaiswal BS, Kljavin NM, Stawiski EW, Chan E, Parikh C, Durinck S, et al. Oncogenic ERBB3 mutations in human cancers. Cancer Cell. 2013 May 13;23(5):603-17.
21. Cheng Y, Li G. Role of the ubiquitin ligase Fbw7 in cancer progression. Cancer Metastasis Rev. 2012 Jun;31(1-2):75-87.
22. Friedlander ML, Russell K, Millis S, Gatalica Z, Bender R, Voss A. Molecular Profiling of Clear Cell Ovarian Cancers: Identifying Potential Treatment Targets for Clinical Trials. Int J Gynecol Cancer. 2016 May;26(4):648-54.
23. Yamamoto S, Tsuda H, Takano M, Tamai S, Matsubara O. Loss of ARID1A protein expression occurs as an early event in ovarian clear-cell carcinoma development and frequently coexists with PIK3CA mutations. Mod Pathol. 2012 Apr;25(4):615-24.
24. Wang YK, Bashashati A, Anglesio MS, Cochrane DR, Grewal DS, Ha G, et al. Genomic consequences of aberrant DNA repair mechanisms stratify ovarian cancer histotypes. Nat Genet. 2017 Jun;49(6):856-65.
25. Yamamoto S, Tsuda H, Takano M, Iwaya K, Tamai S, Matsubara O. PIK3CA mutation is an early event in the development of endometriosis-associated ovarian clear cell adenocarcinoma. J Pathol. 2011 Oct;225(2):189-94.
26. Chandler RL, Damrauer JS, Raab JR, Schisler JC, Wilkerson MD, Didion JP, et al. Coexistent ARI-

D1A-PIK3CA mutations promote ovarian clear-cell tumorigenesis through pro-tumorigenic inflamma-tory cytokine signalling. Nat Commun. 2015 Jan 27;6:6118.

27. Fleuren ED, Zhang L, Wu J, Daly RJ. The kinome 'at large' in cancer. Nat Rev Cancer. 2016 Jan 29;16(2):83-98.

28. Zhang Q, Karnak D, Tan M, Lawrence TS, Morgan MA, Sun Y. FBXW7 Facilitates Nonhomologous End-Joining via K63-Linked Polyubiquitylation of XRCC4. Mol Cell. 2016 Feb 4;61(3):419-33.

29. Lapin V, Shirdel EA, Wei X, Mason JM, Jurisica I, Mak TW. Kinome-wide screening of HER2+ breast cancer cells for molecules that mediate cell proliferation or sensitize cells to trastuzumab therapy. Oncogenesis. 2014 Dec 15;3:e133.

30. Okamoto A, Sehouli J, Yanaihara N, Hirata Y, Braicu I, Kim BG, et al. Somatic copy number alterations associated with Japanese or endometriosis in ovarian clear cell adenocarcinoma. PLoS One. 2015 Feb 6;10(2):e0116977.

31. Tan DS, Iravani M, McCluggage WG, Lambros MB, Milanezi F, Mackay A, et al. Genomic analysis reveals the molecular heterogeneity of ovarian clear cell carcinomas. Clin Cancer Res. 2011 Mar 15;17(6):1521-34.

32. Cohen MH, Williams GA, Sridhara R, Chen G, McGuinn WD,Jr, Morse D, et al. United States Food and Drug Administration Drug Approval summary: Gefitinib (ZD1839; Iressa) tablets. Clin Cancer Res. 2004 Feb 15;10(4):1212-8.

33. Ryan Q, Ibrahim A, Cohen MH, Johnson J, Ko CW, Sridhara R, et al. FDA drug approval summary: lapatinib in combination with capecitabine for previously treated metastatic breast cancer that overex-presses HER-2. Oncologist. 2008 Oct;13(10):1114-9.

34. Posadas EM, Liel MS, Kwitkowski V, Minasian L, Godwin AK, Hussain MM, et al. A phase II and pharmacodynamic study of gefitinib in patients with refractory or recurrent epithelial ovarian cancer. Cancer. 2007 Apr 1;109(7):1323-30.

35. Blank SV, Christos P, Curtin JP, Goldman N, Runowicz CD, Sparano JA, et al. Erlotinib added to carboplatin and paclitaxel as first-line treatment of ovarian cancer: a phase II study based on surgical reassessment. Gynecol Oncol. 2010 Dec;119(3):451-6.

36. Garcia AA, Sill MW, Lankes HA, Godwin AK, Mannel RS, Armstrong DK, et al. A phase II evaluation of lapatinib in the treatment of persistent or recurrent epithelial ovarian or primary peritoneal carcinoma: a gynecologic oncology group study. Gynecol Oncol. 2012 Mar;124(3):569-74.

37. Wilkerson PM, Dedes KJ, Samartzis EP, Dedes I, Lambros MB, Natrajan R, et al. Preclinical evalua-tion of the PARP inhibitor BMN-673 for the treatment of ovarian clear cell cancer. Oncotarget. 2017 Jan 24;8(4):6057-66.

38. Grabiner BC, Nardi V, Birsoy K, Possemato R, Shen K, Sinha S, et al. A diverse array of cancer-as-sociated MTOR mutations are hyperactivating and can predict rapamycin sensitivity. Cancer Discov. 2014 May;4(5):554-63.

39. Farley JH, Brady WE, Fujiwara K, Nomura H, Yunokawa M, Tokunaga H, et al. A phase II evaluation of temsirolimus in combination with carboplatin and paclitaxel followed by temsirolimus consolidation as first-line therapy in the treatment of stage III-IV clear cell carcinoma of the ovary. JCO. 2016 05/20; 2017/11;34(15):5531-.

40. Naing A, Aghajanian C, Raymond E, Olmos D, Schwartz G, Oelmann E, et al. Safety, tolerability, pharmacokinetics and pharmacodynamics of AZD8055 in advanced solid tumours and lymphoma. Br J Cancer. 2012 Sep 25;107(7):1093-9.

41. Mateo J, Olmos D, Dumez H, Poondru S, Samberg NL, Barr S, et al. A first in man, dose-finding study of the mTORC1/mTORC2 inhibitor OSI-027 in patients with advanced solid malignancies. Br J Can-cer. 2016 Apr 12;114(8):889-96.

42. Kashiyama T, Oda K, Ikeda Y, Shiose Y, Hirota Y, Inaba K, et al. Antitumor activity and induction of TP53-dependent apoptosis toward ovarian clear cell adenocarcinoma by the dual PI3K/mTOR inhib-itor DS-7423. PLoS One. 2014 Feb 4;9(2):e87220.

43. Yu P, Laird AD, Du X, Wu J, Won KA, Yamaguchi K, et al. Characterization of the activity of the PI3K/

mTOR inhibitor XL765 (SAR245409) in tumor models with diverse genetic alterations affecting the PI3K pathway. Mol Cancer Ther. 2014 May;13(5):1078-91.

44. Fazio N, Buzzoni R, Baudin E, Antonuzzo L, Hubner RA, Lahner H, et al. A Phase II Study of BEZ235 in Patients with Everolimus-resistant, Advanced Pancreatic Neuroendocrine Tumours. Anticancer Res. 2016 Feb;36(2):713-9.

45. Mehnert JM, Edelman G, Stein M, Camisa H, Lager J, Dedieu JF, et al. A phase I dose-escalation study of the safety and pharmacokinetics of a tablet formulation of voxtalisib, a phosphoinositide 3-kinase inhibitor, in patients with solid tumors. Invest New Drugs. 2017 Apr 17.

46. Adzhubei IA, Schmidt S, Peshkin L, Ramensky VE, Gerasimova A, Bork P, et al. A method and server for predicting damaging missense mutations. Nat Methods. 2010 Apr;7(4):248-9.

47. Kumar P, Henikoff S, Ng PC. Predicting the effects of coding non-synonymous variants on protein function using the SIFT algorithm. Nat Protoc. 2009;4(7):1073-81.

48. Robinson JT, Thorvaldsdottir H, Winckler W, Guttman M, Lander ES, Getz G, et al. Integrative genomics viewer. Nat Biotechnol. 2011 Jan;29(1):24-6.

49. Fehrmann RS, Karjalainen JM, Krajewska M, Westra HJ, Maloney D, Simeonov A, et al. Gene expression analysis identifies global gene dosage sensitivity in cancer. Nat Genet. 2015 Feb;47(2):115-25.

50. Olshen AB, Venkatraman ES, Lucito R, Wigler M. Circular binary segmentation for the analysis of array-based DNA copy number data. Biostatistics. 2004 Oct;5(4):557-72.

51. R D. R: A language and environment for statistical computing. R Foundation for Statistical Computing, Vienna, Austria. 2006.

52. Mermel CH, Schumacher SE, Hill B, Meyerson ML, Beroukhim R, Getz G. GISTIC2.0 facilitates sensitive and confident localization of the targets of focal somatic copy-number alteration in human cancers. Genome Biol. 2011;12(4):R41,2011-12-4-r41. Epub 2011 Apr 28.

53. Cancer Genome Atlas Research Network. Comprehensive genomic characterization defines human glioblastoma genes and core pathways. Nature. 2008 Oct 23;455(7216):1061-8.

54. Wilkerson MD, Hayes DN. ConsensusClusterPlus: a class discovery tool with confidence assessments and item tracking. Bioinformatics. 2010 Jun 15;26(12):1572-3.

55. Alkema NG, Tomar T, Duiker EW, Jan Meersma G, Klip H, van der Zee AG, et al. Biobanking of patient and patient-derived xenograft ovarian tumour tissue: efficient preservation with low and high fetal calf serum based methods. Sci Rep. 2015 Oct 6;5:14495.

56. de Graeff P, Crijns AP, Ten Hoor KA, Klip HG, Hollema H, Oien K, et al. The ErbB signalling pathway: protein expression and prognostic value in epithelial ovarian cancer. Br J Cancer. 2008 Jul 22;99(2):341-9.

57. van der Bilt AR, van der Zee AG, de Vries EG, de Jong S, Timmer-Bosscha H, ten Hoor KA, et al. Multiple VEGF family members are simultaneously expressed in ovarian cancer: a proposed model for bevacizumab resistance. Curr Pharm Des. 2012;18(25):3784-92.

58. Hulsen T, de Vlieg J, Alkema W. BioVenn - a web application for the comparison and visualization of biological lists using area-proportional Venn diagrams. BMC Genomics. 2008 Oct 16;9:488,2164-9-488.

124 OCCC tumors + 47 matched controls

17 OCCC cell lines

Kinome sequencing of:
518 kinases
13 diglyceride kinases
18 PI3K domain & regulatory components
48 cancer related genes

Variant quality minimum:
Mapping quality = 40
Variant location coverage = 10 reads
Variant coverage = 5 reads
Variant read frequency = 10%
Variant read frequency in forward and reverse direction = 5 reads

21892 variants

- Retain only variants with high protein effect probability
- Exclude variants annotated in Exome Variant Server
- Exclude variants present in control samples
- Exclude tumors with low read coverage or alignment (n=2)

1946 variants

- Exclude variants in genes *MIR548N*, *TTN* and *OBSCN*
- Exclude variants in OCCC cell lines
- Exclude variants not confirmed by Haloplex3 sequencing
- In IGV validate genes with a >4% incidence or depicted in oncoprinter illustrations

851 mutations

524 candidate somatic mutations

176 mutations with matched control DNA (somatic mutations)

197 mutations previously annotated as somatic in other in-house kinome sequencing projects
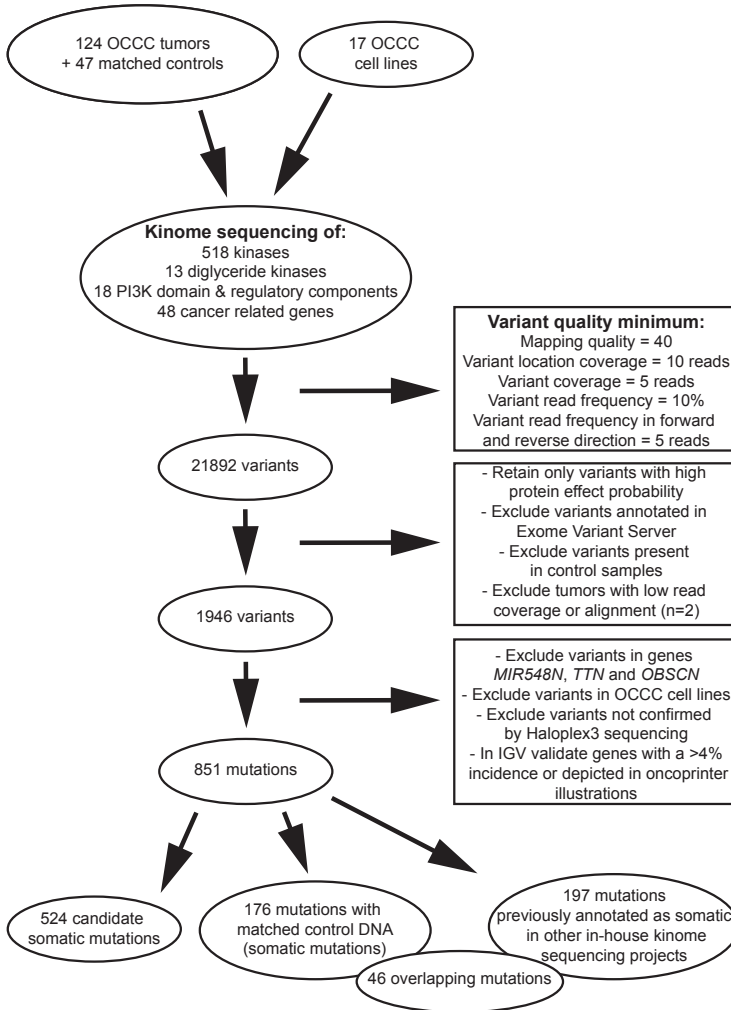
46 overlapping mutations

Figure S1 | Kinome sequencing variant filtering. Pipeline for filtering of kinome sequencing variants.

(**Figure S2** continued legend)
FBXW7, **(E)** *ATM*, **(F)** *CHEK2* and **(G)** *MYO3A* in OCCC. Mutation marks are shown in black (truncating), red (SIFT and PolyPhen damaging prediction), yellow (SIFT or PolyPhen damaging prediction) or white (SIFT and PolyPhen benign prediction). Mutation effects are indicated with a black spot when paired control was available and written in black (previously described mutation) or red (novel mutations).
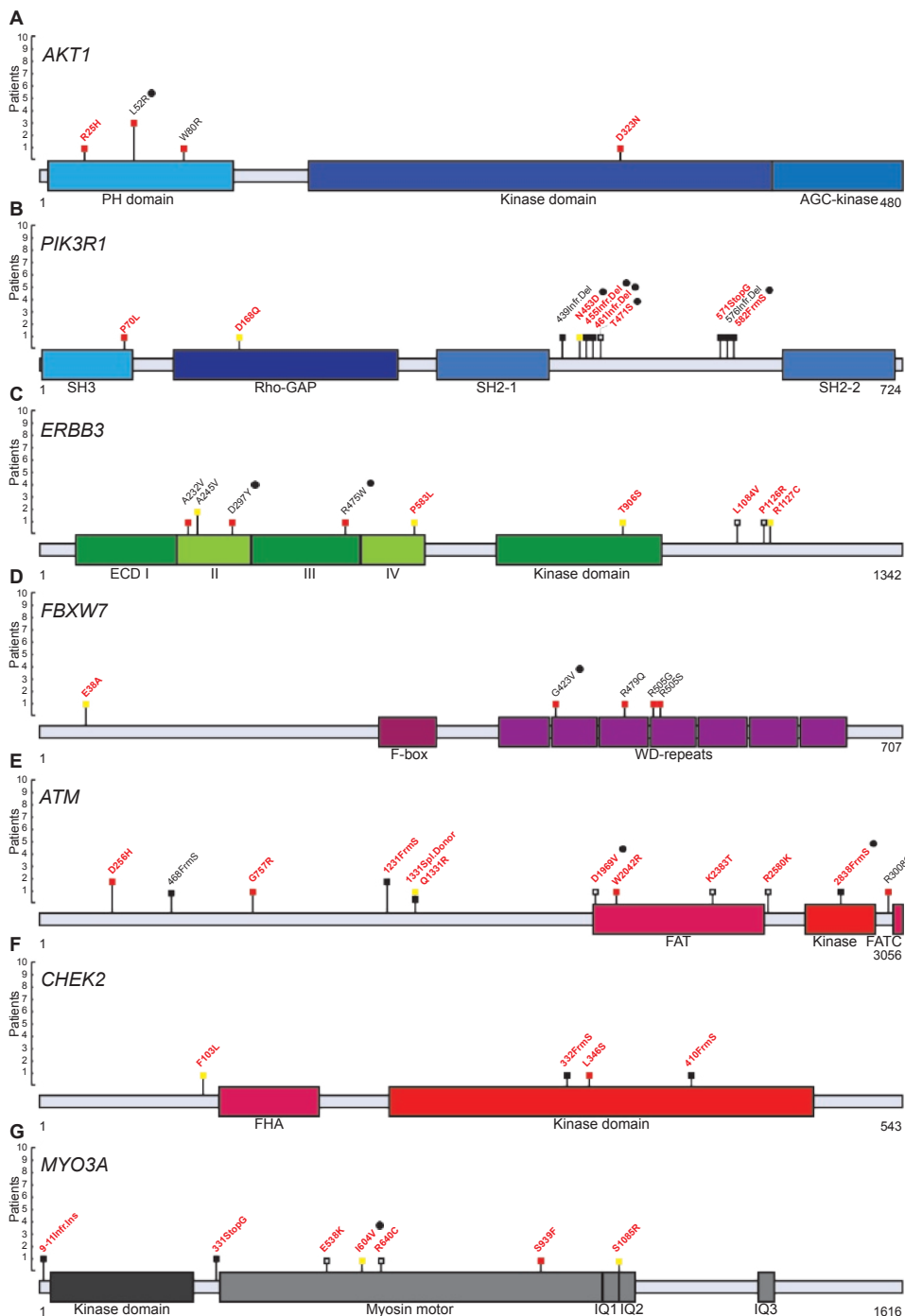
Figure S2 | Significantly mutated genes *AKT1*, *PIK3R1*, *ERBB3*, *FBXW7*, *ATM*, *CHEK2* and *MYO3A*. Schematics of the identified novel significantly mutated genes **(A)** *AKT1*, **(B)** *PIK3R1*, **(C)** *ERBB3*, **(D)** (Legend continued on previous page)
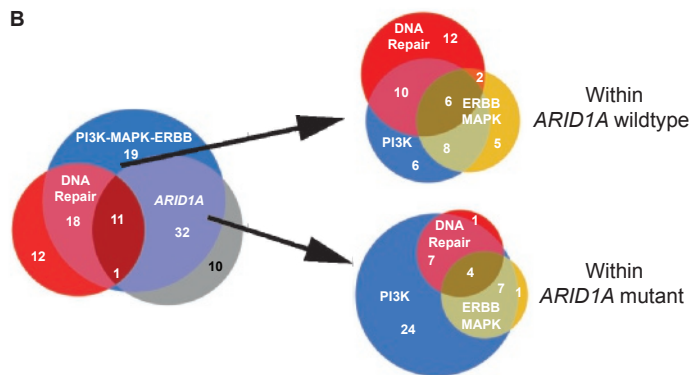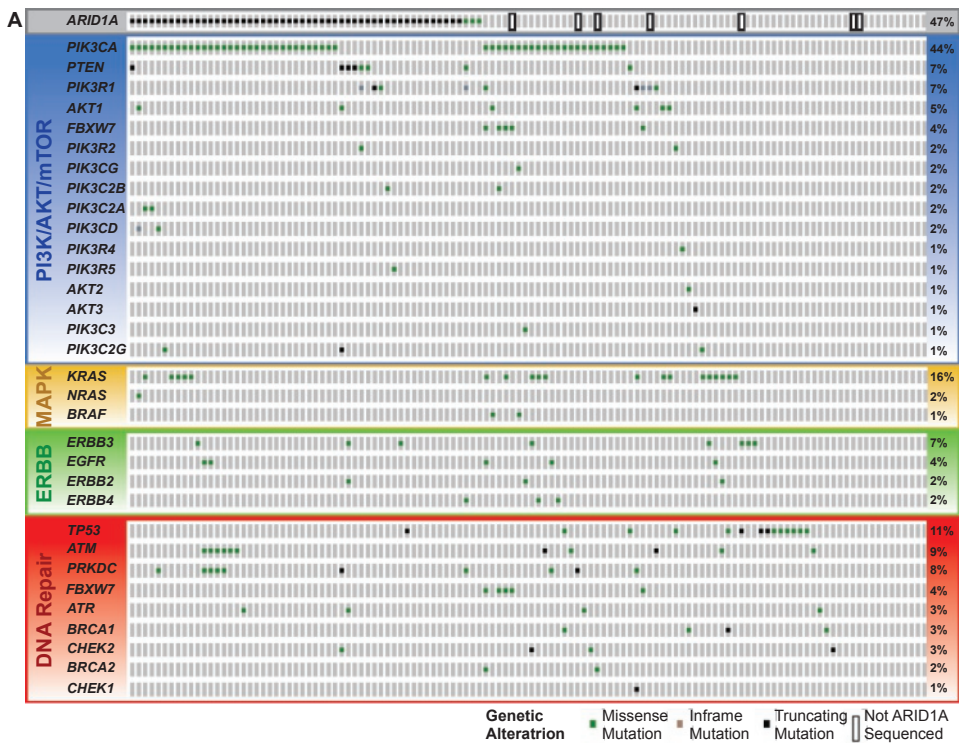
Figure S3 | Mutation distribution in OCCC. (A) Nonsynonymous mutation distribution in genes involved in the frequently mutated PI3K/AKT/mTOR (blue), MAPK pathway (yellow), ERBB family of receptor tyrosine kinases (green) and DNA repair (red) pathway is shown. In this OncoPrint, kinome sequenced OCCC tumors are depicted on the horizontal axis and ordered on mutation frequency in the subsequent altered pathways, represented vertically on the right. *ARID1A* mutant tumors are displayed at the top. **(B)** Bio-Venn diagrams demonstrating overlap in *ARID1A* mutant tumors and PI3K/AKT/mTOR, MAPK and DNA repair pathway and ERBB family of receptor tyrosine kinases mutant tumors (n=103). On the right, PI3K/AKT/mTOR and MAPK pathway, the ERBB family of receptor tyrosine kinases and DNA repair pathway mutations within only *ARID1A* wildtype tumors (n=49) and only *ARID1A* mutant tumors (n=44) are shown. All data in A and B is derived from 122 kinome-sequenced OCCC tumors, overlap in BioVenn diagram circles is proportional to group overlap.
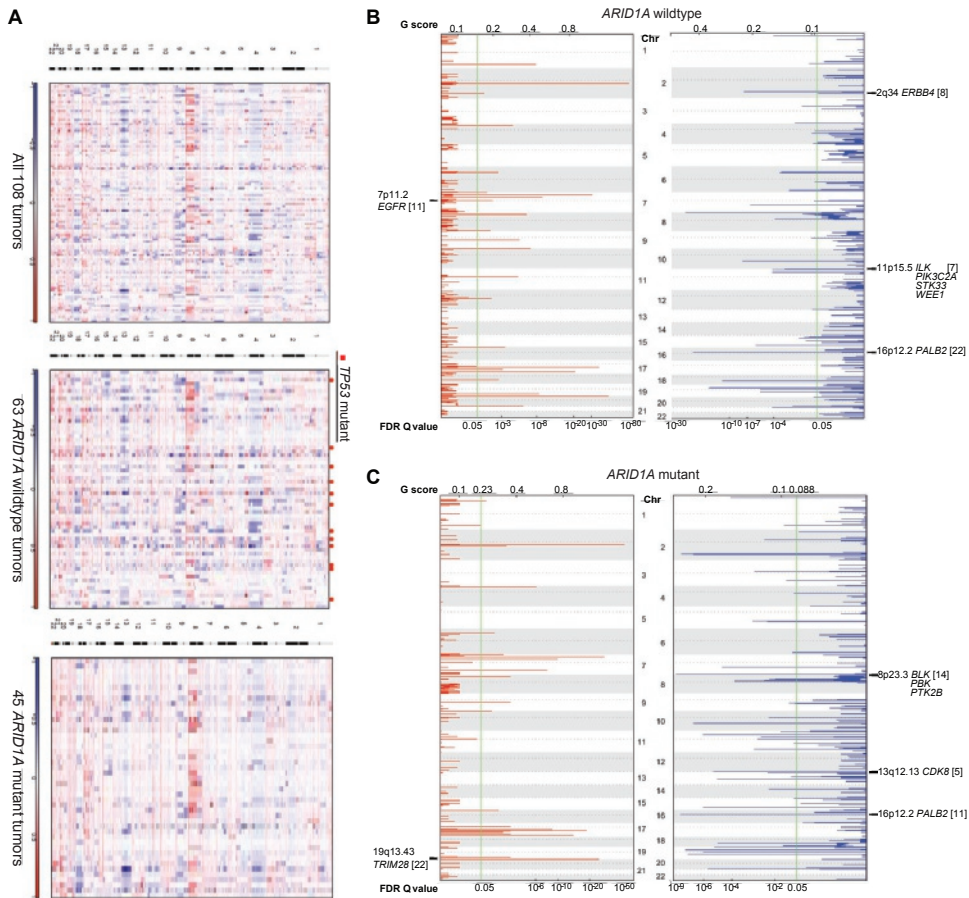
Figure S4 | Whole genome CNA heatmap. (A) Genome-wide CNA heatmap profiles of all 108 OCCC tumors (above), 63 *ARID1A* wildtype tumors (middle) and 45 *ARID1A* mutant tumors (below). **(B)** Significant CNA plot of only *ARID1A* wildtype tumors (n=63) and **(C)** only *ARID1A* mutant tumors (n=45) as determined by GISTIC analysis. All kinases and cancer-related genes from the kinome sequencing gene panel that were focally significantly amplified (red) or deleted (blue) are indicated along the chromosomes vertically. Chromosomal location and total amount of tumors harboring the event are annotated with each gene name. False-discovery rate (FDR) 0.05 threshold, indicated by the green line, and G-score are shown along the horizontal axis.

Figure S5 | Clustering (n=106) and survival analysis (n=70) on kinome mutations and CNA. (A) Disease-specific survival of patients (n=70) grouped on *ARID1A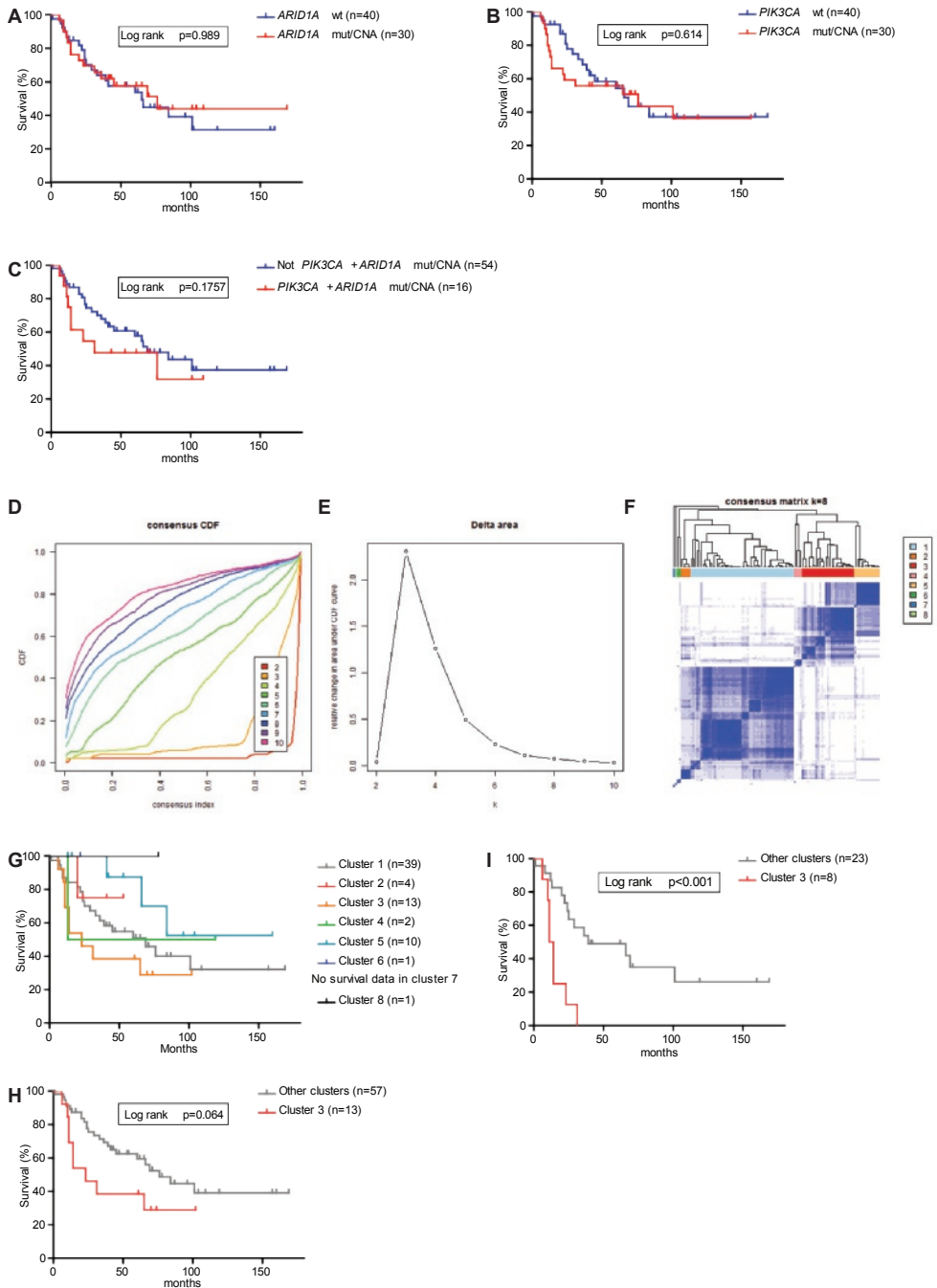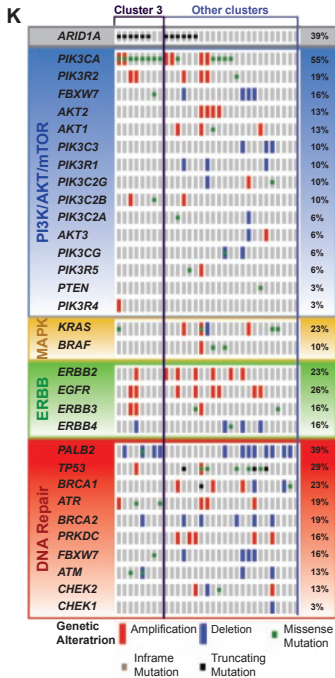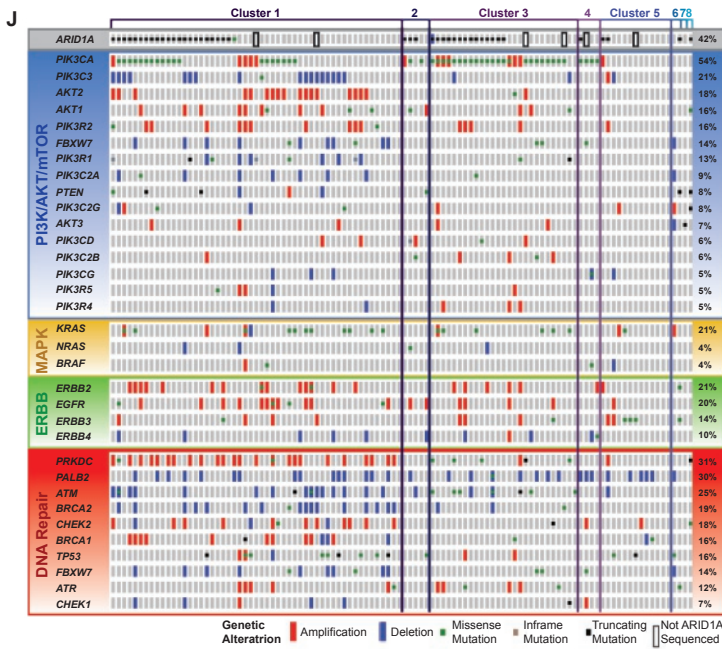* status, **(B)** *PIK3CA* status and **(C)** *ARID1A* + *PIK3CA* status. **(D)** Consensus clustering, with maximum group count set to 10 and cluster-

Cluster 1 | **2** | **Cluster 3** | **4** | **Cluster 5** | **678**

PI3K/AKT/mTOR — ARID1A 42%, PIK3CA 54%, PIK3C3 21%, AKT2 18%, AKT1 16%, PIK3R2 16%, FBXW7 14%, PIK3R1 13%, PIK3C2A 9%, PTEN 8%, PIK3C2G 8%, AKT3 7%, PIK3CD 6%, PIK3C2B 6%, PIK3CG 5%, PIK3R5 5%, PIK3R4 5%

MAPK — KRAS 21%, NRAS 4%, BRAF 4%

ERBB — ERBB2 21%, EGFR 20%, ERBB3 14%, ERBB4 10%

DNA Repair — PRKDC 31%, PALB2 30%, ATM 25%, BRCA2 19%, CHEK2 18%, BRCA1 16%, TP53 16%, FBXW7 14%, ATR 12%, CHEK1 7%

Genetic Alteratrion — Amplification | Deletion | Missense Mutation | Inframe Mutation | Truncating Mutation | Not ARID1A Sequenced

K

Cluster 3 | **Other clusters**

ARID1A 39%

PI3K/AKT/mTOR — PIK3CA 55%, PIK3R2 19%, FBXW7 16%, AKT2 13%, AKT1 13%, PIK3C3 10%, PIK3R1 10%, PIK3C2G 10%, PIK3C2B 10%, PIK3C2A 6%, AKT3 6%, PIK3CG 6%, PIK3R5 6%, PTEN 3%, PIK3R4 3%

MAPK — KRAS 23%, BRAF 10%

ERBB — ERBB2 23%, EGFR 26%, ERBB3 16%, ERBB4 16%

DNA Repair — PALB2 39%, TP53 29%, BRCA1 23%, ATR 19%, BRCA2 19%, PRKDC 16%, FBXW7 16%, ATM 13%, CHEK2 13%, CHEK1 3%

Genetic Alteratrion — Amplification | Deletion | Missense Mutation | Inframe Mutation | Truncating Mutation

ing optimization with 1000 repetitions maximum, shows adding of tumors (n=106) as consensus index (horizontally) and empirical cumulative distribution (vertically) for 1-10 clusters. **(E)** Area under the curve plot of decrease in friction from 1-10 clusters. **(F)** Heatmap distribution of tumors in 8 clusters. **(G)** Disease-specific survival of patients (n=70) in 8 clusters, **(H)** cluster 3 vs. other clusters. **(I)** Disease-specific survival in advanced stage OCCC patients (FIGO 2C-4), Log rank (Mantel-Cox) was used for statistical analysis. **(J)** Nonsynonymous mutation distribution in genes involved in the frequently mutated PI3K/AKT/mTOR (blue) and MAPK pathway (yellow), ERBB family of receptor tyrosine kinases (green) and DNA repair pathway (red) as well as *ARID1A* and *PALB2* are shown with OncoPrint. CNA in each mutated gene are added. The 106 OCCC tumors that were both kinome sequenced and SNP arrayed are shown on the horizontal axis grouped on tumor clusters and ordered on total event frequency in the subsequently altered pathways. **(K)** Oncoprint from advanced stage patients in cluster 3 vs. other clusters, shown on the horizontal axis grouped on tumor clusters and ordered on total event frequency in the subsequent altered pathways, ordered as aforementioned.
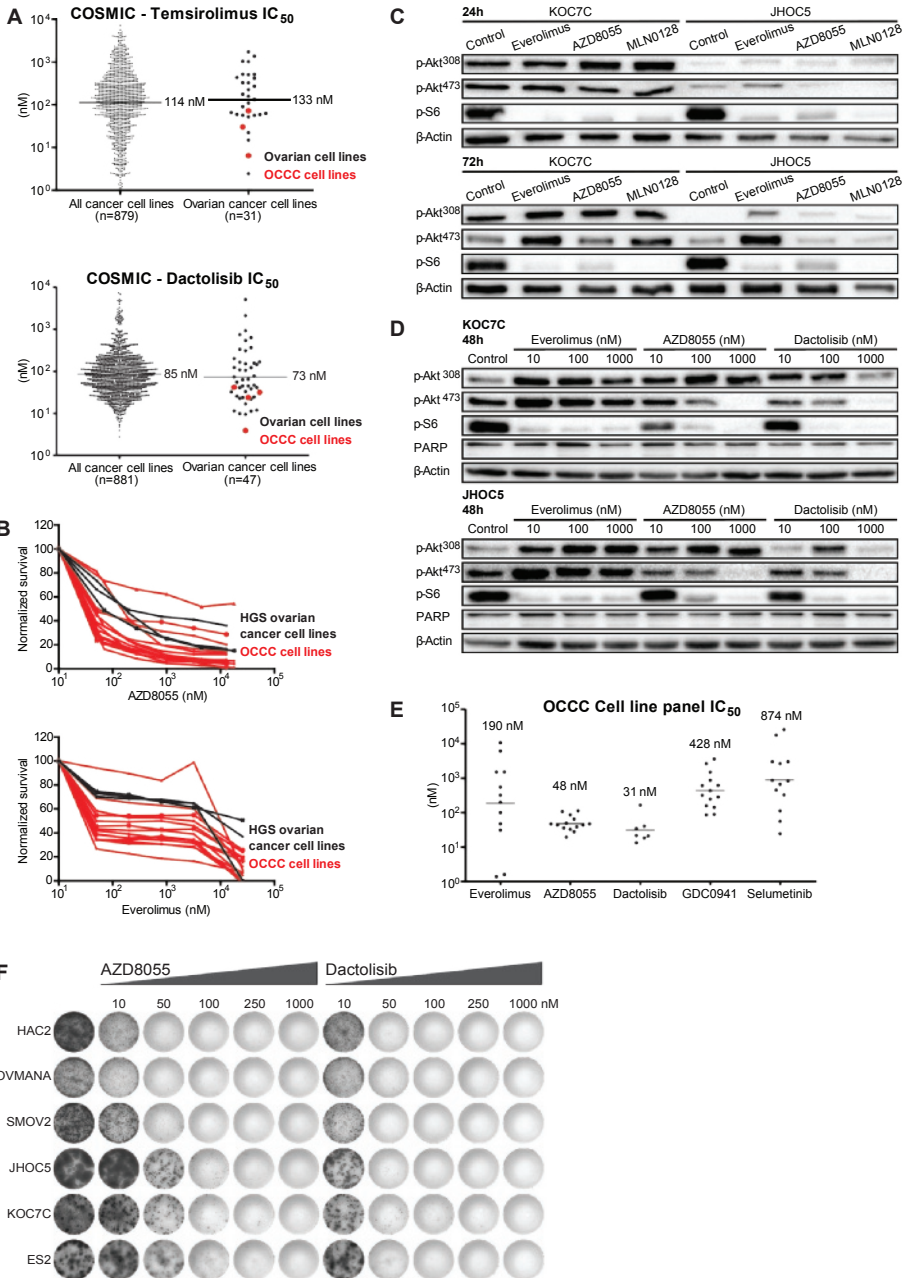
Figure S6 | mTORC1, mTORC1/2 and PI3K-mTORC1/2 inhibitor sensitivities. (A) IC_{50} of the mTORC1 inhibitor temsirolimus and dactolisib from COSMICs drug screening database in all cancer cell lines vs. ovarian cancer cell lines, horizontal lines indicate geometric mean. **(B)** MTT assay curves from AZD8055 (above) or everolimus (below) treatment on the aforementioned cell line panel. **(C)** Expression of p-AKT[308], p-AKT[473] and p-S6 after 24 (up) and 72h (down) exposure to 100 nM everolimus, AZD8055 or MLN0128 (Legend continued on next page)

in the OCCC cell lines KOC7C or JHOC5 determined by Western blot. β-Actin was used as loading control. Results are representative from n=2 experiments. **(D)** Expression of p-AKT[308], p-AKT[473], p-S6 and (cleaved) PARP after 48h exposure to increasing concentrations of everolimus, AZD8055 and dactolisib in the OCCC cell lines KOC7C (up) and JHOC5 (down) determined by Western blot. β-Actin was used as loading control. Results are representative from n=2 experiments. **(E)** Everolimus, AZD8055, GDC0941 and selumetinib IC_{50} determined for 14 OCCC cell lines (ES2, KOC7C, SMOV2, JHOC5, RMG1, OVMANA, HAC2, OV207, OVTOKO, TOV21G, OVAS, OVCA429, TUOC1 and RMG2) and dactolisib IC_{50} determined for seven OCCC cell lines (ES2, KOC7C, SMOV2, JHOC5, RMG1, OVMANA and HAC2) by MTT assay. Selumetinib IC_{50} of KOC7C was not reached at maximum used concentration of 25 uM. Horizontal lines indicate geometric mean. Data is derived from n≥2 experiments. **(F)** Long-term proliferation assay after exposure to increasing concentrations of AZD8055 and dactolisib. Results are representative from n=3 experiments.
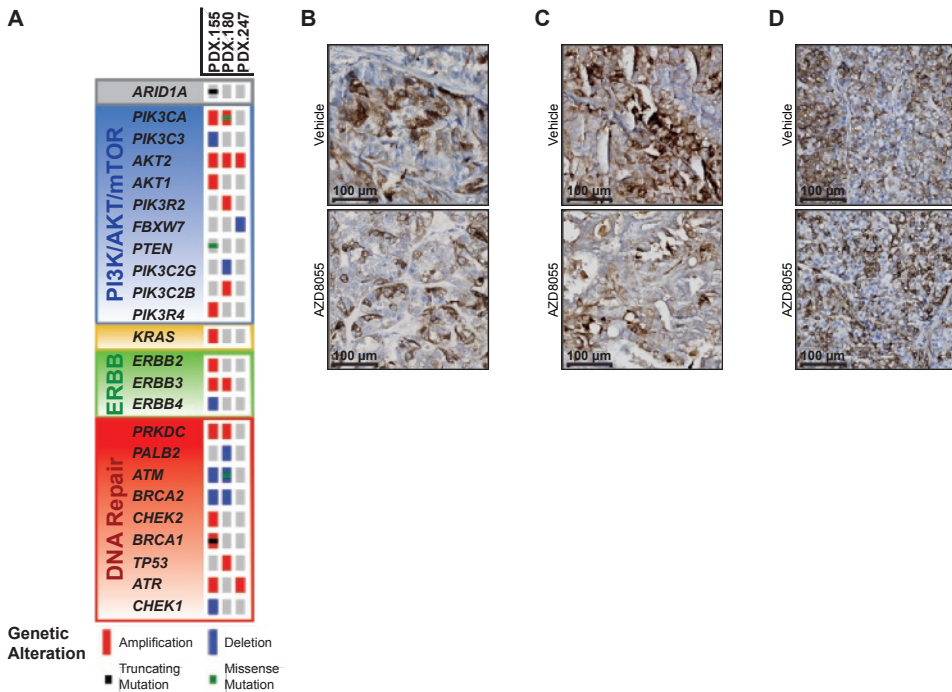
Figure S7 | PDX alteration status and p-S6 staining. (A) Nonsynonymous mutation distribution in PDX.155, PDX.180 and PDX.247 in genes involved in the frequently mutated PI3K/AKT/mTOR (blue), MAPK pathway (yellow), ERBB family of receptor tyrosine kinases (green) and DNA repair pathway (red) as well as *ARID1A* and *PALB2* are shown with OncoPrint. CNA in each mutated gene are added. **(B)** PDX.155, **(C)** PDX.180 and **(D)** PDX.247 representative p-S6 expression after 21 days of vehicle or AZD8055 treatment.

Table S1 | Gene set for kinome sequencing. All human kinases (n=518) and a set of customly selected genes including PI3K domain proteins (n=12), diglyceride kinases (n=13), PI3K regulatory components (n=6) and additional cancer related genes (n=48). Full gene list is available as supplementary table online.

Table S2 | Gene set for Haloplex sequencing.

	Gene ID	ENSMBL		Gene ID	ENSMBL
1	ARID1A	ENST00000324856	21	BRD2	ENST00000374825
2	SMARCA4	ENST00000590574	22	PKN1	ENST00000242783
3	PIK3CA	ENST00000263967	23	PRKCQ	ENST00000263125
4	PIK3R1	ENST00000521381	24	PRPF4B	ENST00000337659
5	PTEN	ENST00000371953	25	MYO3B	ENST00000408978
6	AKT1	ENST00000555528	26	BRCA1	ENST00000357654
7	KRAS	ENST00000311936	27	BRCA2	ENST00000544455
8	ERBB3	ENST00000267101	28	TRRAP	ENST00000359863
9	EGFR	ENST00000275493	29	NRAS	ENST00000369535
10	TP53	ENST00000269305	30	BRAF	ENST00000288602
11	ATM	ENST00000278616	31	ERBB2	ENST00000269571
12	ATR	ENST00000350721	32	EIF2AK4	ENST00000263791
13	CHEK2	ENST00000382580	33	LRRK2	ENST00000298910
14	SGK223	ENST00000622241	34	WNK2	ENST00000297954
15	FES	ENST00000328850	35	TAF1	ENST00000423759
16	MYO3A	ENST00000265944	36	ERBB4	ENST00000342788
17	PRKDC	ENST00000314191	37	CTNNB1	ENST00000396183
18	MAST4	ENST00000403625	38	SMAD4	ENST00000398417
19	FBXW7	ENST00000281708	39	STK11	ENST00000326873
20	CAMK2B	ENST00000395749	40	MET	ENST00000318493

Table S3 | Binomial testing of kinome sequencing variants.

	Gene	patients affected	Gene size (bp)	p-value
1	PIK3CA	54	4196	9.58E-46
2	KRAS	19	4320	0.00011
3	TP53	14	2280	0.00024
4	PTEN	8	4560	0.00082
5	AKT1	6	3554	0.00429
6	PIK3R1	9	7320	0.00437
7	FBXW7	5	2986	0.00914
8	ERBB3	7	6360	0.01930
9	ATM	11	12720	0.02070
10	CHEK2	4	2520	0.02258
11	MYO3A	7	7440	0.03975
12	ARAF	4	3341	0.05368
13	ERN2	5	4911	0.05798
14	PHKG2	3	2129	0.06152
15	EIF2AK4	6	6600	0.06210
16	PIM2	3	2280	0.07224
17	SBK2	2	1080	0.07613
18	MYC	3	2400	0.08130
19	PBK	3	2400	0.08130
20	IRS2	4	4200	0.10230

Table S4 | Clinicopathological characteristics (n=70 patients).

Clinicopathological characteristics

	All patients (n=70)	
	N	*%*
Age (years)[a]	56 (29-81)	
Missing	11	
FIGO stage		
1	36	51.4
2	7	10
3	24	34.3
4	3	4.3
Surgery		
Complete debulking	61	87.1
Incomplete debulking	7	12.9
Type of chemotherapy		
No chemotherapy	5	7.1
Platinum based	11	15.7
Platinum/taxane based	45	64.3
Other regimen	8	11.4
Missing	1	1.4

[a] Data is expressed as median (range).

Abbreviations: FIGO, International Federation of Gynaecology and obstetrics.